FLUID FLOW ANALYSIS OF LOW-ALTITUDE AGRICULTURAL UAV PESTICIDE SPRAYING DEVICE

HAN DAN

FACULTY OF ENGINEERING
UNIVERSITY OF MALAYA
KUALA LUMPUR

2020

FLUID FLOW ANALYSIS OF LOW-ALTITUDE AGRICULTURAL UAV PESTICIDE SPRAYING DEVICE

HAN DAN

THESIS SUBMITTED IN FULFILMENT OF THE REQUIREMENTS FOR THE DEGREE OF MASTER OF MECHANICAL ENGINEERING

FACULTY OF ENGINEERING
UNIVERSITY OF MALAYA
KUALA LUMPUR

2020

UNIVERSITY OF MALAYA

ORIGINAL LITERARY WORK DECLARATION

Name of Candidate: Han Dan

Matric No: KQK180043

Name of Degree: Master of mechanical engineering

Title of Project Research Report: Fluid flow analysis of low-altitude agricultural pesticide spraying device UAV

Field of Study: Mechanical design, CFD

I do solemnly and sincerely declare that:

(1) I am the sole author/writer of this Work;
(2) This Work is original;
(3) Any use of any work in which copyright exists was done by way of fair dealing and for permitted purposes and any excerpt or extract from, or reference to or reproduction of any copyright work has been disclosed expressly and sufficiently and the title of the Work and its authorship have been acknowledged in this Work;
(4) I do not have any actual knowledge nor do I ought reasonably to know that the making of this work constitutes an infringement of any copyright work;
(5) I hereby assign all and every rights in the copyright to this Work to the University of Malaya ("UM"), who henceforth shall be owner of the copyright in this Work and that any reproduction or use in any form or by any means whatsoever is prohibited without the written consent of UM having been first had and obtained;
(6) I am fully aware that if in the course of making this Work I have infringed any copyright whether intentionally or otherwise, I may be subject to legal action or any other action as may be determined by UM.

Candidate's Signature Date:

Subscribed and solemnly declared before,

Witness's Signature Date:

Name:

Designation:

FLUID FLOW ANALYSIS OF LOW-ALTITUDE AGRICULTURAL UAV PESTICIDE SPRAYING DEVICE

ABSTRACT

The nozzle is an important part of the drone pesticide spraying device. The quality of the nozzle directly affects the atomization performance. Fan nozzles are widely used in the field of plant protection in agriculture, forestry, pest control, and weed removal. When using drones to spray pesticides, the spraying velocity, the spraying range of the pesticides, and the atomized particle size are all key factors that directly affect the efficiency of pesticide use. This paper uses SOLIDWORKS and ANSYS software to design and simulate. The boundary conditions are kept the same, and the influence of the nozzle's grooving angle (α), nozzle cavity diameter (D), and nozzle throat length (L) on fluid velocity, pressure, and mass flow is measured. Then, this project report compares and studies the influence of the changes of different structural parameters on the internal flow field of the combined flat fan nozzle, and find the influence relationship between different structural parameters and nozzle atomization performance; and the best structure corresponding to the nozzle with the optimal atomization performance parameter combination. Pesticide residues and droplet drift are minimized to reduce pesticide waste and environmental pollution.

The research observes the pressure and velocity distribution of the fluid flow inside the nozzle. By comparing the results concluded that the fluid flows from the nozzle inlet to the nozzle outlet, the pressure of the flow field inside the nozzle gradually decreases, and the velocity gradually increases. The pressure and velocity at the nozzle groove vary the most. The grooving angle of the nozzle has the greatest influence on the fluid velocity and spraying range. The cavity diameter and grooving angle of the fan nozzle have the greatest influence on the mass flow. The nozzle cavity diameter and throat length have a small effect on fluid velocity. The shape and droplet quality of the spray of the combined

flat fan nozzle is better than the flat fan nozzle. The simulation results of 13 combined flat fan nozzles are compared and analyzed comprehensively, and the nozzle structure parameters are combined as follows: the nozzle with the parameters of α=35°, d=3mm, l=2mm has the best atomization performance out of the 13 nozzles.

Keywords: Flat fan nozzle; Mechanical design; ANSYS FLUENT; Computational fluid dynamics

FLUID FLOW ANALYSIS OF LOW-ALTITUDE AGRICULTURAL UAV PESTICIDE SPRAYING DEVICE

ABSTRAK

Muncung adalah bahagian penting dari alat penyembur racun perosak drone. Kualiti muncung secara langsung mempengaruhi prestasi pengabusan. Muncung kipas banyak digunakan dalam bidang perlindungan tanaman di bidang pertanian, perhutanan, pengendalian hama, dan penyingkiran rumpai. Semasa menggunakan drone untuk menyemburkan racun perosak, kecepatan penyemburan, jarak penyemburan racun perosak, dan ukuran zarah atom adalah semua faktor utama yang secara langsung mempengaruhi kecekapan penggunaan racun perosak. Makalah ini menggunakan perisian SOLIDWORKS dan ANSYS untuk merancang dan mensimulasikan. Keadaan batas tetap sama, dan pengaruh sudut alur muncung (α), diameter rongga muncung (D), dan panjang kerongkong muncung (L) pada halaju, tekanan, dan aliran jisim bendalir diukur. Kemudian, laporan projek ini membandingkan dan mengkaji pengaruh perubahan parameter struktur yang berbeza pada medan aliran dalaman muncung kipas rata gabungan, dan mencari hubungan pengaruh antara parameter struktur yang berbeza dan prestasi atomisasi muncung; dan struktur terbaik yang sesuai dengan muncung dengan kombinasi parameter prestasi atomisasi yang optimum. Sisa residu racun perosak dan pengaliran titisan diminimumkan untuk mengurangkan sisa racun perosak dan pencemaran alam sekitar.

Penyelidikan ini memerhatikan tekanan dan halaju aliran aliran bendalir di dalam muncung. Dengan membandingkan hasil yang disimpulkan bahawa bendalir mengalir dari saluran masuk muncung ke saluran keluar muncung, tekanan medan aliran di dalam muncung secara beransur-ansur menurun, dan kecepatan secara beransur-ansur meningkat. Tekanan dan halaju pada alur muncung sangat berbeza. Sudut lekukan muncung mempunyai pengaruh terbesar pada halaju bendalir dan jarak penyemburan.

Diameter rongga dan sudut alur muncung kipas mempunyai pengaruh terbesar pada aliran jisim. Diameter rongga muncung dan panjang tekak mempunyai pengaruh kecil terhadap halaju bendalir. Bentuk dan kualiti titisan semburan muncung kipas rata gabungan lebih baik daripada muncung kipas rata. Hasil simulasi 13 muncung kipas rata gabungan dibandingkan dan dianalisis secara komprehensif, dan parameter struktur muncung digabungkan seperti berikut: muncung dengan parameter $\alpha = 35\ °$, d = 3mm, l = 2mm mempunyai prestasi atomisasi terbaik daripada 13 muncung.

Kata kunci: Muncung kipas rata; Reka bentuk mekanikal; FLUENT ANSYS; Pengiraan dinamik bendalir

ACKNOWLEDGEMENTS

Firstly, I want to sincerely thank my supervisor Dr. Farazila Binti Yusof, who provided a lot of help during my project research. With her professional academic scholarship and rich research experience, she has given me great support, encouragement, and help for my subject research. I would also like to thank Dr. Nik Nazri Bin Nik Ghazali for his patient explanation of computational fluid dynamics. He can always give me complex knowledge in a way that is easy to understand. The rigorous scientific research, persevering work spirit and serious attitude of the two professors are a model for my study, and let me realize that no matter whether it is living or studying, I must treat it seriously, which will inspire me in my future work and go forward seriously and down-to-earth in life. When the project is completed, I hereby express my sincere thanks and high respect to all the teachers who have helped and taught me.

I also want to thank my friends Barry, Kevin, and William. They are both my classmates and my roommates, for their care and help in my study and life. They made me feel a sincere friendship.

Special thanks to the University of Malaya for giving me the opportunity to learn mechanical engineering expertise.

TABLE OF CONTENTS

LIST OF FIGURES

LIST OF TABLES

LIST OF SYMBOLS AND ABBREVIATIONS

UAV	:	Unmanned Aerial Vehicle
h	:	Distance from pore to edge
H	:	Depth of notch
e	:	Eccentric distance
α	:	Grooving angle
D	:	Cavity diameter
L	:	Nozzle throat length
Hr	:	Relative cutting depth
r	:	The radius of curvature of the nozzle end shape
g	:	Gravitational acceleration
ρ	:	Liquid density
P	:	Liquid pressure
μ	:	Flow coefficient
k	:	Turbulent kinetic energy
ε	:	Turbulent dissipation rate
σ_k	:	Prandtl number of turbulent kinetic energy
σ_ε	:	Prandtl number of dissipation rate of turbulent kinetic energy
G_k	:	Turbulent kinetic energy caused by laminar velocity gradient
C_ε	:	Turbulent kinetic energy caused by laminar velocity gradient
A	:	Area section of the pipe

LIST OF APPENDICES

CHAPTER 1: INTRODUCTION

1.1 Introduction to low-altitude agricultural UAV pesticide spraying device

Traditional agricultural spraying relies mostly on manual pesticide or tractor spraying in the field with handheld devices. The disadvantages of traditional spraying devices include high labor intensity, low efficiency, and high demand for human resources. In the process of traditional pesticide spraying, it is easily affected by weather and terrain. These factors will cause damage to crop and fail to increase the productivity of crops, especially in developing countries (RaoMogili, 2018). Many countries in the world have begun to study the use of low-altitude drones instead of traditional artificial pesticide spraying. Since the drone has the characteristics of stable flight speed, it can hover in the air, with no professional take-off and landing airport is required, and the downward airflow generated by the drone's wings can increase the penetration of pesticides, so low-altitude drones pesticide spraying system has become a hot research in many countries. In 1912, Canada began to use airplanes as an auxiliary tool to spray pesticides on field crops and orchards. In 1918, the United States used airplanes to spray insecticides for the first time to prevent locust plagues (Tan Luke, 2014). After more than 30 years of development in Japan, the development of agricultural plant protection drones and pesticide application technology has gradually matured. It can be filled with gasoline and medicine in a short time. The pesticide application efficiency is very high. Aerial spraying of drones has huge application potential in many parts of Asia (Xinyu Xue, 2016).

The three main factors for preventing pests through chemical technology are plant protection machinery, pesticides, and pesticide application technology. In plant protection machinery, the performance of the atomizing nozzle directly affects the working efficiency of pesticides. The type, structure, material, workmanship, and other factors of the atomization nozzle are directly related to the quality of the atomization. Among the many types of nozzles, fan nozzles are currently the most widely used nozzles. The fan

nozzle has a simple structure, low processing cost, and can be used on many occasions. Compared with traditional nozzles, fan nozzles have higher droplet adhesion and are easier to control. Therefore, the fan nozzle can reduce the harm of pesticides to non-target crops caused by the deviation. It is important to research the effect of the structural parameters of fan nozzles on the spray velocity, internal pressure, and mass flow rate of the nozzle. This article studies the effects of combined flat fan nozzles and flat fan nozzles with different parameter structures on fluid velocity and pressure. The low-altitude agriculture UAV pesticide device as follows:

Figure 1.1:UAV Pesticide Spraying Device (JENSEN, 2019)

1.2 Problem Statement

Choosing an inappropriate type of nozzle will cause pesticides to float and deposit during the spraying process. This will reduce the efficiency of pesticide use, causing damage to crop, and even damaging the non-target crops. There is not much difference in the internal structure of the flat fan nozzle and the combined flat fan nozzle. Their spray shapes are difficult to distinguish. It can be a confusing task to choose the most suitable nozzle. On the other hand, the spray velocity and the mass flow rate of pesticides are also

important factors affecting pesticide spraying efficiency. At present, there are few studies on the influence of nozzle grooving angle, cavity diameter, and throat length on spray performance.

1.3 Objectives

The objectives of this project are the influence of the structural parameters of the flat fan nozzle on the spray performance, which can provide a theoretical basis and experimental data for grasping the relationship between the fan nozzle structures and the spray performance. This research provides a theoretical basis for the design and application of flat fan nozzles.

(1) The simulation analyzes the influence of the grooving angle, cavity diameter, and throat length of the combined flat fan nozzle on the spray performance of the UAV spraying pesticide device, then summarizes the parameters of the best performance combined flat fan nozzle.

(2) The simulation analyzes and compares the spray velocity and mist distribution of the combined flat fan and flat fan nozzles, then summarizes the spray shapes and characteristics of the two kinds of nozzles.

1.4 Scope

This project mainly studies the spray distribution of combined flat fan nozzles and flat fan nozzles, and the influence of different terminal shapes on spray performance. The modeling is performed by SOLIDWORKS software, and the ANSYS FLUENT software is used to calculate fluid dynamics. Through the simulation results, the spray velocity and mass flow of fan nozzles with different parameter structures are compared. In this way, the relationship between the grooving angle, the diameter of the cavity, and the length of the throat on the spray performance can be found.

1.5 Outline

This dissertation consists of five chapters:

Chapter 1: The agricultural drone pesticide spraying device and the role of the flat fan nozzle in the agricultural drone pesticide spraying device are introduced. State the main problems of the flat fan nozzle research and the objectives of this research. And literature review of previous research.

Chapter 2: This chapter focuses on the literature review on the types of pressure nozzles, the main parameters of the flat fan nozzle and the atomization process of the fan nozzle. The introduction of diaphragm pump and pesticide.

Chapter 3: This chapter gives a detailed description of the designed fan nozzles structure parameters and simulation methods. Which includes governing equations, mesh, Reynolds number calculation, and turbulence model.

Chapter 4: The experimental results of the simulation are shown in the form of tables and figures. The influence of grooving angle, cavity diameter, and throat length on liquid velocity, pressure and quality is discussed.

Chapter 5: This chapter summarizes the conclusions based on the experimental results and make suggestions for future work.

CHAPTER 2: LITERATURE REVIEW

2.1 Background

In agricultural production, pesticides are essential. The principle of using pesticides is to spray them to reach the target crops. Make the target crop grow faster or prevent the target crop from being damaged by pests. These pesticides are then broken down into harmless substances (Snelder DJ, 2008). The traditional pesticide spraying process is carried out by workers using hand-held spraying devices. Workers are exposed to high concentrations of pesticides. Once agricultural workers inhale, ingest, or come into contact with the skin of pesticides, it will cause harm to the workers' bodies (Lesmes Fabian C, 2014). Of the three routes, skin contact is the most common method (Acquavella JF, 2004). Every year, many workers in the agricultural sector die because of the harm of pesticides. Therefore, the risk faced by pesticide workers is very high (Kearney GD, 2015). According to the World Health Organization, there are around 3 million insecticide poisoning incidents worldwide each year(Wang Bin, 2016). In Malaysia, people's awareness of pesticide hazards is not high. The main reason is that information about pesticide hazards is rarely reported. The mass media hardly report information about chemical pollution and pesticide poisoning (Mourin, 2002). The most used herbicide in Malaysia is paraquat. However, paraquat can cause toxicity and harm to the human body. The government banned it until 2002 (Shariff FM, 2008).

On the one hand, to solve the harm of pesticides to the health of agricultural workers, countries around the world have begun to use drone pesticide spraying devices to replace traditional manual pesticide spraying. Agricultural personnel can remotely control the flight path of the drone, avoiding direct contact with pesticides (Y. Huang, 2009). On the other hand, UAVs have the characteristics of stable flight speed, low-altitude flight, vertical take-off, and landing. Unmanned aerial vehicles are not restricted by terrain and

can complete some more difficult tasks. The efficiency of pesticide spraying is much higher than traditional manual spraying. Therefore, the drone pesticide spraying device is a very worthy project (Vikrant Suryawanshi, 2019).

In the drone pesticide spraying device, the performance of the nozzle directly affects the use efficiency of pesticides (Zhai Enyu, 2013). The shape of the spray is usually decided by the terminal shape of the nozzle hole (Yang Xuejun, 2005). The process of the combined fan nozzle is the liquid flows in the hemispherical nozzle inlet through the throat, and then is ejected from the "V"-shaped incision, and the liquid spreads on the axis of the V-shaped incision. The spray shape of a fan nozzle is usually a fan. Fan-shaped nozzles with different internal structures have different spray shapes (Lu Xiaolan, 2011). The research on the structural parameters of fan-shaped nozzles generally uses experimental testing methods, which require different test platforms and methods, and the development cost is high (Wang Yanping, 2009). Therefore, the purpose of this research is to compare fan nozzles of UAV pesticide spraying devices with different structural parameters through FLUENT simulation analysis.

2.2 Introduction of flat fan nozzle

2.2.1 Types of pressure spray nozzles

The pressure is applied to the pesticide through the pump and then sprayed out from the fan pressure nozzle. The diameter of the droplet of the liquid medicine is generally 70-120 microns. The advantage of the pressure nozzle is that the liquid medicine has higher pressure, strong penetrating power, and the amount of liquid medicine produced is small, and the evaporation in arid areas is small; the disadvantage of the pressure nozzle is that the liquid medicine is not uniformly atomized and the droplet diameter is a difference, and the nozzle is easy to block, especially when spraying powder (Qingni, 2011).

In today's agricultural production, the pressure nozzles often used for pesticide spraying mainly include fan nozzles, straight nozzles, full cone nozzles, and hollow cone nozzles. For the fan nozzles, the shape of spray is fan shaped. For the straight nozzles, the shape of spray is a straight line. The spray shape of a full cone nozzle is a filled circle and a hollow cone nozzle spray shape is a hollow circle. Agricultural engineer Bobby Grisso and David Holshur agronomist drew schematic diagrams of the mist shapes of flat fan nozzles, hollow cone nozzles, and full cone nozzles. The shape of different kinds of nozzles mist distribution as follows:

Figure 2.1The shape of flat fan nozzle mist distribution (Holshouser, 2013)

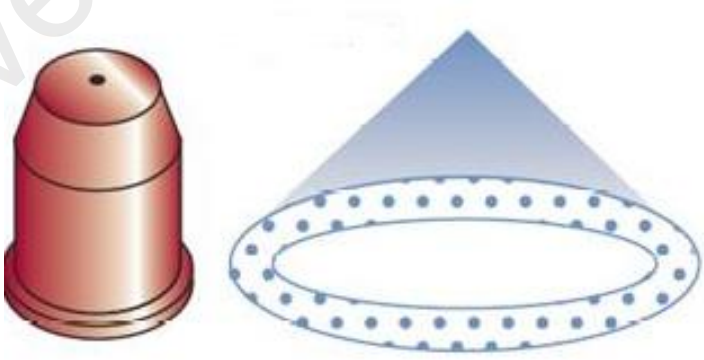

Figure 2.2: The shape of hollow cone nozzle mist distribution (Holshouser, 2013)

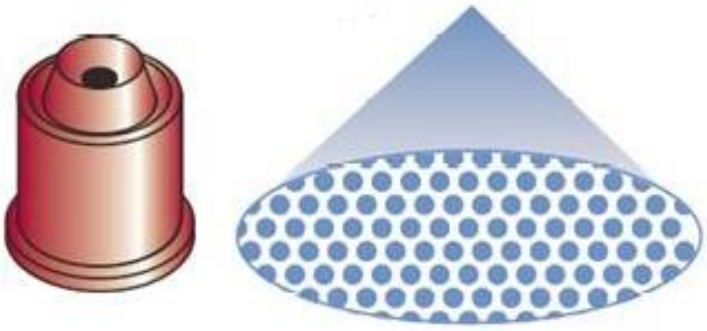

Figure 2.3: The shape of full cone nozzle mist distribution (Holshouser, 2013)

The working path of the low-altitude drone spraying device is to travel in a straight line to realize the uniform spraying of pesticides by surrounding the farmland. Therefore, the drone spray device is suitable for using fan nozzles. The fan nozzle can ensure uniform spraying of pesticides and low droplet drift. The following details the types of fan nozzles. Fan nozzles can be divided into many types according to capacity, spray angle, and material. Standard fan nozzles are uniformly represented by the 'J' code. According to different flow rates, they can be divided into low flow flat fan nozzles, standard capacity flat fan nozzles, and large capacity flat fan nozzles. Standard flat fan nozzles are available in a wide range of different capacities, spray angles, thread sizes, and materials (Junhua, 2018). Common fan nozzles include narrow-angle nozzles, wide-angle nozzles, combined flat fan nozzles, single fan nozzles, self-cleaning fan nozzles, flat fan nozzles, dovetail fan nozzles, clip-on fan nozzles, quick removal fan nozzles, side Spray fan nozzle, general fan nozzle (Huijiang, 2011). The standard fan nozzle is liquid column flow or fan spray, which can produce high impact force. The spray of the nozzle is evenly distributed. The droplet size is small to medium (Xiang, 2014). The combined fan nozzles and flat fan nozzles studied in this project are standard flat fan nozzles. The picture comes from the combined flat fan and flat fan nozzles produced by LORRIC.

Figure 2.4: Combined flat fan nozzle (LORRIC, 1991)

Figure 2.5:Flat fan nozzle (LORRIC, 1991)

2.2.2 Characteristics and materials of flat fan nozzle

Fan nozzle is a nozzle commonly used in agricultural pesticide spraying devices. Because it has better atomization performance under low intake pressure. There are many

spray angles options, uniform spray distribution, good atomization performance, and both large flow and small flow liquid spraying work can be used. Therefore, this article focuses on the atomization characteristics of the flat fan nozzle. The fan nozzle has a simple structure and low processing cost. When the drone is working, the flying altitude is usually not too high. According to the survey, the working height of plant protection drones is generally 2-4 meters (Wang Yanping, 2009). Plant protection drones work at low altitudes, and a larger spray angle is required at low altitudes, which can improve work efficiency. The working path of the plant protection drone is straight forward flight. Therefore, the spray shape of the fan nozzle is very suitable for plant protection drones. The spray shape of the cone nozzle is circular. If the cone nozzle is used on a plant protection drone, uneven spraying will occur, which will cause phytotoxicity. The combined flat fan nozzle consists of a throat, a hemispherical head, and a "V" shaped outlet nozzle. The flat fan nozzle is a combination of a cylindrical throat and a "V" shaped outlet nozzle. The internal structure of the two nozzles is not much different, and the main structural parameters are the same.

The materials used for fan nozzles are usually stainless steel, brass, plastic, etc. The material of the nozzle determines the corrosion resistance and wear resistance of the nozzle (Fan Rong, 2016).

2.2.3 The atomization process of the fan nozzle

The atomization process of the liquid in the fan nozzle is the liquid is delivered into the nozzle by the pressure generated by the pump. The liquid is pressed against the wedge-shaped inside surface of the nozzle outlet groove. When the pressure is large enough, the liquid film spreads, and the liquid film becomes thinner. Finally, the liquid is subdivided into droplets by pressure, and then evenly sprayed on the crops (Burguete J, 2003). When the flow rate of the nozzle increases, the film of viscoelastic fluid thickens and eventually

becomes unstable and atomizes into droplets. The water film produced by the flat fan nozzle has the most unstable edge of the fluid, and when the viscoelasticity of the fluid increases, the stability of the film produced by the nozzle increases, thereby promoting the flow rate of the fluid film. However, beyond the critical flow rate for film rupture, the number of holes in the film and the growth rate increase, accelerating the further refinement of the droplets. (Thompson J C, 2007)

The quality of spray is mainly affected by many factors such as natural factors, agronomic conditions, and sprayer technology (Fan Qingni, 2010). Spray distribution rules: Spray distribution of the nozzle depends on the nozzle terminal shape, surface roughness, verticality, parallelism, symmetry, and position errors that will affect the amount of spray. This article researches the influence of the structural parameters of the flat fan nozzle on the atomization performance. Simulation results through ANSYS FLUENT software. Then compared the influence of grooving angle, cavity diameter, and throat length on liquid mass flow, velocity, and pressure.

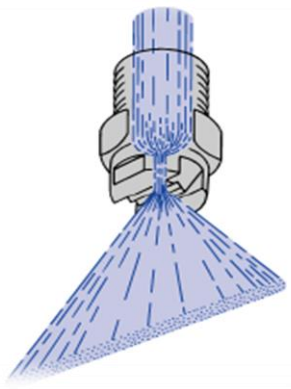

Figure 2.6: The atomization process of the fan nozzle (Huang, 2014)

2.3 Diaphragm pump

A diaphragm is a positive displacement pump. The diaphragm pump can increase the suction power of the liquid, so its output efficiency is high. The internal structure of the diaphragm pump can separate the liquid from the fragile part of the pump, so it has a long

service life. The fan nozzle can have better atomization performance under low-pressure conditions. The applicable pressure range of the pressure fan nozzle is 2-4 bar (Organization, 2003). This means that the working pressure of the pump should be 0.2-0.4 Mpa. Therefore, this study chose the Yanmis brand 12v diaphragm pump. Its maximum working pressure is 300000 pascals. Diaphragm pumps use a combination of the reciprocating action of rubber, thermoplastic or Teflon diaphragms and suitable valves (check valves, butterfly valves, discs or some form of shut-off valve) on both sides of the diaphragm to pump liquids (Diaphragm pump, 2008). The types of diaphragm pumps are low-pressure pump, low flow pump and high flow pump. This is determined by the effective working diameter and strokes length of the diaphragm. Diaphragm pumps can be used for the transportation of alcohol, pesticides, and various liquid drugs.

Figure 2.7: Diaphragm pump (Yanmis, 2019)

Table 2.1:Specification of diaphragm pump

Voltage	Maximum power	Maximum pressure	Working pressure	Opening flow	Weight
12V	15W	500000 pascals	300000 pascals	$0.000025 m^3/s$	608g

2.4 Introduction to pesticide

Pesticides are chemicals used to prevent harmful insects from destroying crops, control the growth environment of crops, and regulate plant production (United States Environmental Protection Agency, 2018). Pesticides can be simply divided into herbicides used to improve the production environment of crops and pesticides used to regulate plant growth according to their different functions. The quality of spray drops is related to the performance of pesticides. Viscosity is one of the important factors. Surfactant molecules in the liquid squeeze and collide under pressure to generate viscous force. The higher the viscosity of the liquid is more difficult to atomize and narrower the spray angle (Wiles-Purdue, 2020). Therefore, when using higher viscosity pesticides, pumps with higher working pressure should be used. This article uses water as the cell zone condition because water and pesticides are both incompressible liquids and most pesticides used in agriculture are diluted with water.

2.5 Previous studies

Zhang Xinming researched the effects of the main structural parameters of the high-pressure fan nozzle, such as the shrinkage angle β, the ratio of length, and the eccentric distance L/e, and the grooving angle on the spray performance. The study uses the three-dimensional Navier-Stokes equations as the governing equations, uses the standard k-ε turbulence model to establish a governing equation set, and uses CFD FLUENT software to establish a three-dimensional model of the internal flow field of the fan nozzle. The conclusion of the grooving angle is that the grooving angle has better clustering when the grooving angle is 15°-30°, but it has a certain influence on the spray velocity; the grooving angle of 30°-45° can get a better spray velocity. While the grooving angle is 45°-60°, although high spray velocity can be obtained, the jet clustering is poor (Zhang Xinming, 2012).

Hou Junhua performed internal fluid flow simulations on flat fan nozzles, combined flat fan nozzles and ball head fan nozzles. The selected parameters of the research institute are the range of grooving angle 15°-30°, the cavity diameter 1.5mm-2.5mm. The standard k-ε turbulence model is used, and the solution method is SIMPLE. It is concluded that the nozzle atomization performance is the best when the groove angle is 30° and the cavity diameter is 2.5mm. The internal flow field of the combined flat fan nozzle is more stable (Junhua, 2018).

2.5.1 Summary

In previous simulation studies of fluid flow in the nozzle, researchers have used the standard k-ε turbulence model and SIMPLE solution method. This shows that the standard k-ε turbulence model and SIMPLE solution method are accurate and appropriate in the simulation of the fluid flow problem inside the nozzle. The range of parameters used in previous studies is small, and there is no research on the influence of structural parameters on liquid mass flow. This paper has more parameter data and calculated the influence of different structural parameters on mass flow.

CHAPTER 3: METHODOLOGY

3.1 Introduction

In this chapter, the main parameter structure of the fan nozzle is introduced, and the structural parameters of the combined fan nozzle are designed to research the influence of different structural parameters on spray efficiency. The grooving angle, cavity diameter, and throat length is selected as variable parameters. Five groups of control groups were made for each parameter. The grooving angle is selected 15°, 25°, 35°, 45°, 60°. The cavity diameter is selected 1mm, 1.5mm, 2mm, 2.5mm, 3mm. The throat length is selected 2mm, 3mm, 4mm, 5mm, 6mm. The Standard $\boldsymbol{k-\varepsilon}$ turbulence model is used to simulate the velocity and pressure distribution of the liquid.

3.2 Research flow chart

The research process is as follows:

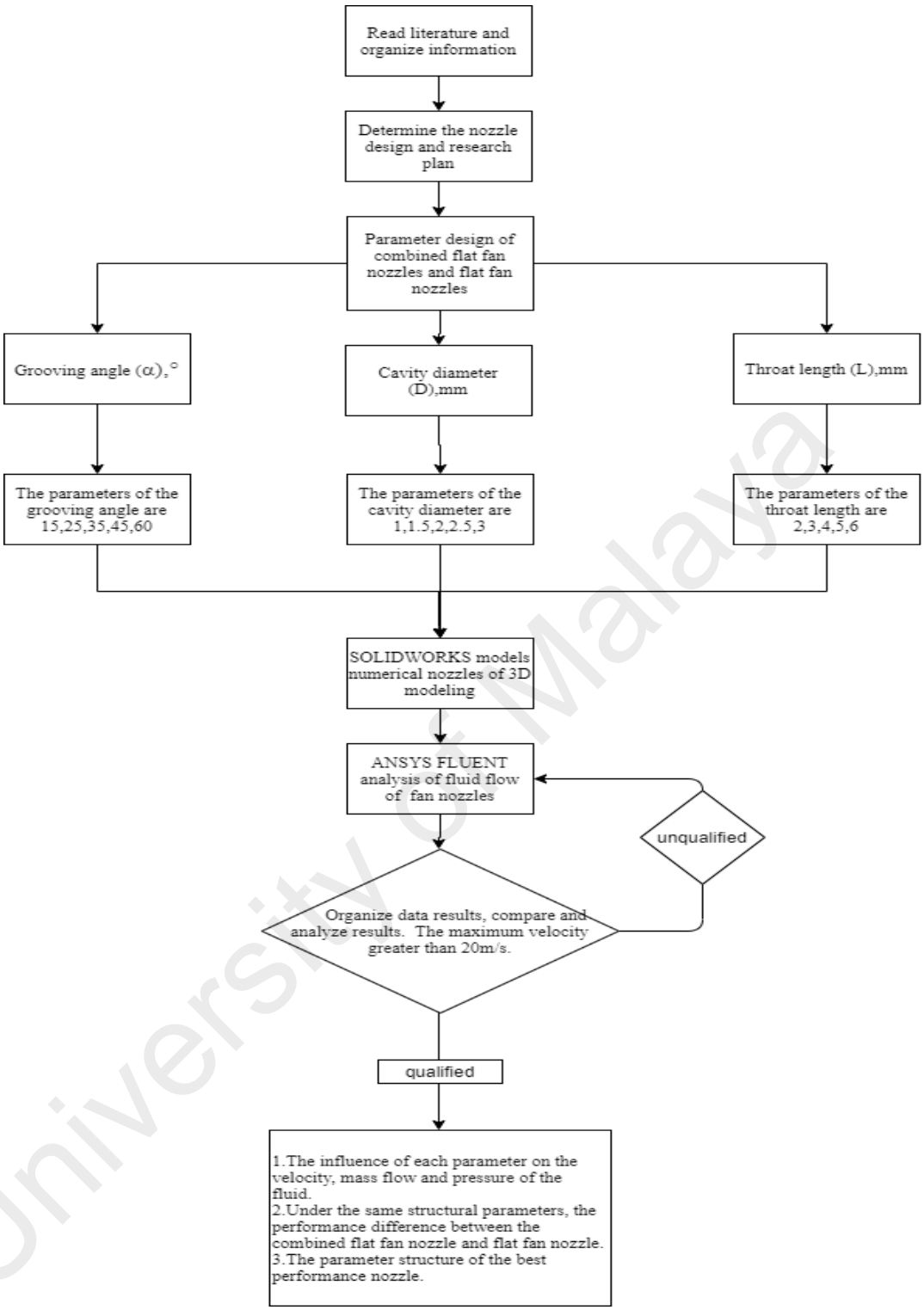

Figure 3.1:research flow chart

3.3 Design of fan nozzles

3.3.1 Introduction

The modeling software in this article chooses to use SOLIDWORKS, SOLIDWORKS is a powerful and convenient 3D drawing software. It is found on the

data provided by the user and the set condition parameters to accurately establish the user's expected model. SOLIDWORKS has three main modules, which are part modeling module, part assembly module and engineering drawing module. Because the nozzle is a one-part model, the fan flat nozzle can be modeled using the part modeling module. SOLIDWORKS can dynamically modify the features and sketches of the established model. This can greatly shorten the operation time in the design process. SOLIDWORKS can also transfer data to other engineering software, such as PRO/E, UG and ANSYS. This article uses SOLIDWORKS modeling 13 kinds of combined flat fan nozzles and one kind of different terminals in the shape of a fan nozzle in the 3D model. The figure below shows a 3D model of a combined fan nozzle with the grooving angle equal to 35°, the cavity diameter equal to 2mm, and the throat length equal to 3mm.

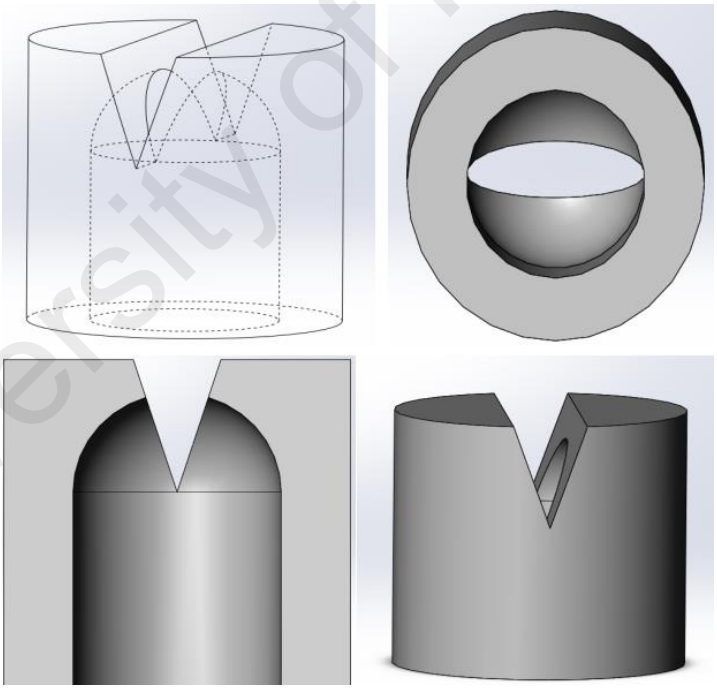

Figure 3.2: 3D model of combined flat fan nozzle

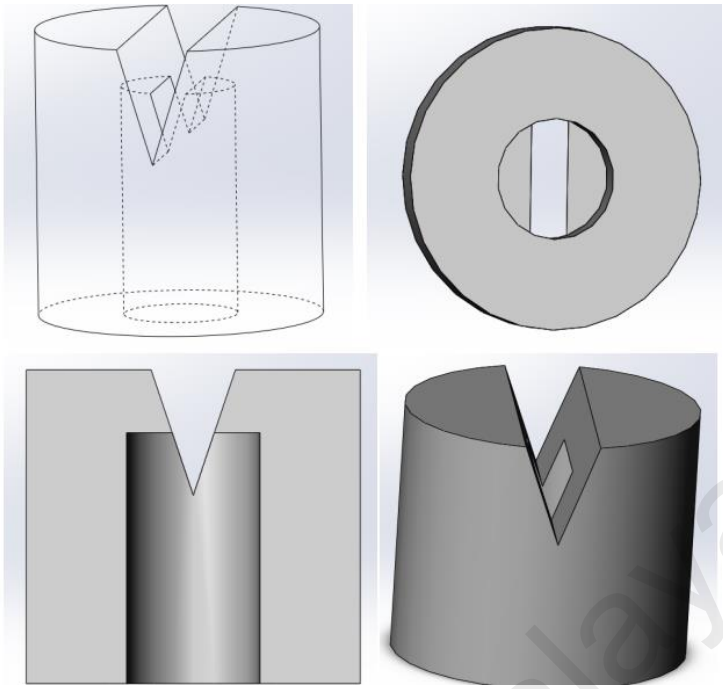

Figure 3.3: 3D model flat fan nozzle

3.3.2 Main parameters of fan nozzle structure

The structural parameters of the fan nozzle mainly include grooving angle α, cavity diameter D, throat length L, and relative cutting depth Hr. The equation for calculating the relative depth of cut as flow:

$$Hr = \frac{r - e}{r} = \frac{H - h}{r} \quad (1)$$

The relative cutting depth Hr between 0.5 and 1.5 is more appropriate (Junhua, 2018). When the relative cutting depth is greater than 1.5, the structural size of the whole nozzle increases, causing material wasted. When the relative cutting depth Hr is less than 0.5, the atomization performance will be reduced. Therefore, the relative cutting depth of the nozzle designed in this paper is 1. Calculated from equation 3.1, when Hr is equal to 1, the eccentric distance e is must equal to 0. Depth of notch H equal to cavity diameter D. The distance from pore to edge equal to the radius of curvature of the nozzle end shape r.

The main parameters of the combined flat fan nozzle are shown in the Figure3.4:

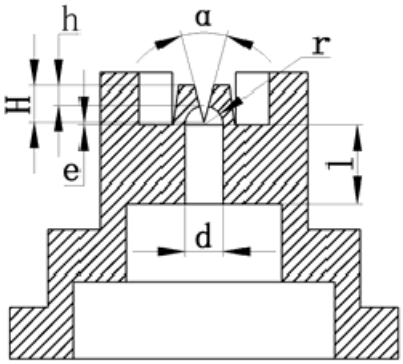

Figure 3.4: Internal structural parameters of flat fan nozzle

h=Distance from pore to edge

H=Depth of notch

e= Eccentric distance

α=Grooving angle

D= Cavity diameter

L= Nozzle throat length

Hr=Relative cutting depth= $\frac{r-e}{r} = \frac{H-h}{r}$

r= The radius of curvature of the nozzle end shape

Considering the technology of machining, the nozzle cavity diameter should not be too small, the smallest nozzle cavity diameter should be bigger than or equal to 1.0 mm. The Stress intensity increased pressure will increase, while the area increases pressure decreases, and under the condition of constant pressure. In order to reduce energy consumption, so should reduce the cavity diameter. Therefore, the cavity diameter of the nozzle is chosen 1mm to 3mm. The grooving angle generally ranges from 10 ° to 90 ° (Li

Xu, 2000). Therefore, the 3D model design uses SOLIDWORKS software to build a model including the top part of the fan nozzle, the throat, and the V-shaped wedge outlet.

Modeling was carried out for the three factors of the combined flat fan nozzle changing the grooving angle, the nozzle throat length, and the diameter of the cavity. The grooving angles are selected 15°, 25°, 35°, 45°, 60°. The cavity diameters are selected 1mm, 1.5mm, 2mm, 2.5mm, 3mm. The throat lengths are selected 2mm, 3mm, 4mm, 5mm, 6mm. To research the influence of every parameter on the spray performance of the fan nozzle. All model structural parameters are shown in the Table3.1:

Table 3.1: Structural parameters of the fan nozzle of the experimental group

Nozzle No.	α (°)	D (mm)	L(mm)
1	15	2	3
2	25	2	3
3	35	2	3
4	45	2	3
5	60	2	3
6	35	1	3
7	35	1.5	3
8	35	2.5	3
9	35	3	3
10	35	3	2
11	35	3	4
12	35	3	5
13	35	3	6

The first group is the No.1, No2, No3, No4, No5 model. The objective is analyzing the influence of the grooving angle on the spray performance under the condition of keeping

the cavity diameter and throat length unchanged. The second group is the No.6, No.7 No.3，No.8，No.9 model. The second group is to analyze the influence of the Cavity diameter on the spray performance under the condition of keeping the grooving angle and throat length unchanged. The third group is the No.10, No.9, No.11, No.12, No.13 model. The third group is to analyze the influence of throat length on spray performance under the condition of keeping the grooving angle and cavity diameter unchanged.

3.3.3 Fluid flow analysis of fan nozzle

This paper uses the workbench and software in ANSYS FLUENT software to simulate the internal structure of the nozzle and analyze the fluid flow. The American company ANSYS designed the general-purpose finite element analysis software. It can be matched with many design software to allow data sharing, such as NASTRAN and Auto CAD (Ou Qibin, 2016). The range of applications is very wide, involving many different fluid phenomena. Computational fluid dynamics (CFD) technology for high-speed aerodynamics and methods for solving incompressible turbulent flows in mechanical and civil engineering.

According to the principle of fluid mechanics and Bernoulli's equation, the spray volume Q is equal to the product of the liquid velocity v and the cross-sectional area F of the nozzle outlet (Jianming, 2005).

$$Q = \mu \cdot F = \mu \sqrt{2g\frac{p}{\rho}} \cdot F \tag{2}$$

g= gravitational acceleration (N/kg)

ρ= liquid density

p= liquid pressure

μ=flow coefficient

The flow coefficient μ is an important parameter for calculating flow, the calculate method as follow:

$$\mu = \frac{1}{\sqrt{1+\sum \mu}} \tag{3}$$

$\sum \mu$ is the sum of the shrinkage coefficient of the nozzle section, which is determined by the structural parameters of the nozzle. The result calculated by the formula alone will have a relatively large error with the actual situation, and the corresponding correction calculation must be carried out through experiments to obtain a more reasonable value of the flow coefficient. Finally, the relationship between the flow rate and the flow coefficient can be fitted based on the experimental data. It can be known that the main structural parameters that affect the spray volume of the fan nozzle are the nozzle cavity diameter D, the grooving angle α and the nozzle throat length L (Pingzeng, 2007).

3.4 Governing equations

The continuity equation is a specific formula of the law of conservation of mass in fluid mechanics.

Continuity equation:

$$\frac{\partial \rho}{\partial t} + \frac{\partial}{\partial x_i}(\rho \mu_i) = S_m \tag{4}$$

$$\frac{\partial}{\partial x_i}(\rho \mu_i) = \frac{\partial(\rho \mu)}{\partial x} + \frac{\partial(\rho v)}{\partial y} + \frac{\partial(\rho \omega)}{\partial z} = 0 \tag{5}$$

Where ρ is the density, t is time and μ, v, ω are velocity vector in the x, y, z direction (Pedlosky, 1987).

In this paper, the fluid medium in the simulation analysis of the flow field inside the nozzle is water, which can be regarded as incompressible fluids ($\frac{\partial \rho}{\partial t} = 0$). Therefore, the governing equation of mass conservation can be simplified as Equation:

$$\frac{\partial(\rho\mu)}{\partial x} + \frac{\partial(\rho v)}{\partial y} + \frac{\partial(\rho\omega)}{\partial z} = 0 \tag{6}$$

Navier-Stokes equation, in fluid mechanics, a partial differential equation that describes the flow of incompressible fluids. The equation is a generalization of the equation devised by Swiss mathematician Lds.eonhard Euler in the 18th century to describe the flow of incompressible and frictionless fluids (Augustyn, 2011), the Equation as follow :

$$\frac{\partial \mu}{\partial t} + \mu \cdot \nabla\mu = -\frac{\nabla p}{\rho} + \upsilon\nabla^2\mu \tag{7}$$

Where μ is the fluid velocity vector, P is the fluid pressure,ρ is the fluid density, υ is the kinematic viscosity, and ∇^2 is the Laplacian operator.

3.5 Simulation conditional

3.5.1 Mesh

Save the modeling with SOLIDWORKS. Save the file as x_t format. Open the x_t file with ANSYS and open the model in the geometry of the FLUID FLOW module. For the accuracy of simulation results, edge sizing is added to the model. Element order is linear, and the solver preference is fluent. Because each model has different structural parameters, the volume and surface area are also different. The range of element size was set between 0.085mm with 0.12mm. Choose high-quality smoothing. The statistics element is around 500,000. Because of ANSYS version problems, ANSYS will not be able to calculate more than 512,000 structural elements.

3.5.1.1 Meshing of combined flat fan nozzle

Select ‘face’ in the options. Select the face that the nozzle inlet and outlet. Open the named selections option and add inlet and outlet. Then update the mesh.

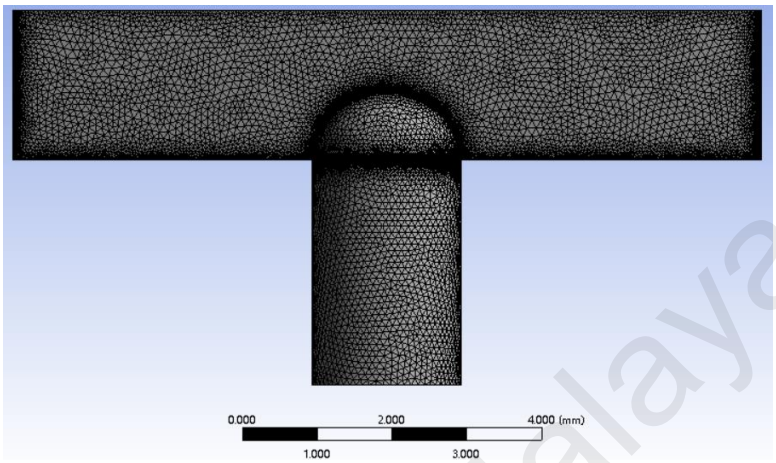

Figure 3.5:The front view of the mesh

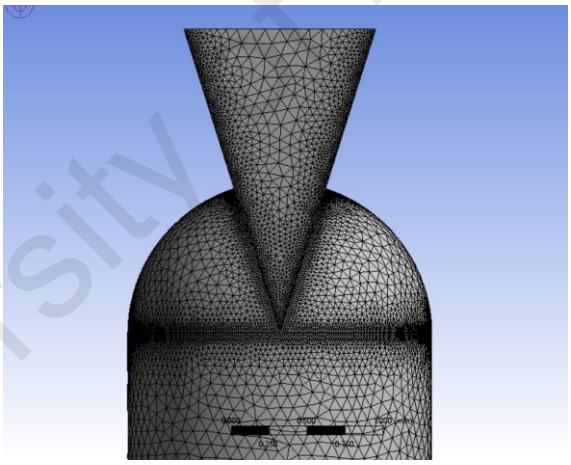

Figure 3.6:The left view of mesh

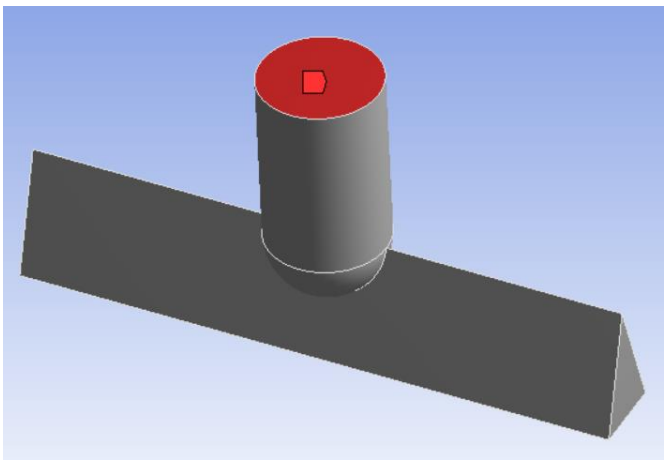

Figure 3.7:Inlet of nozzle

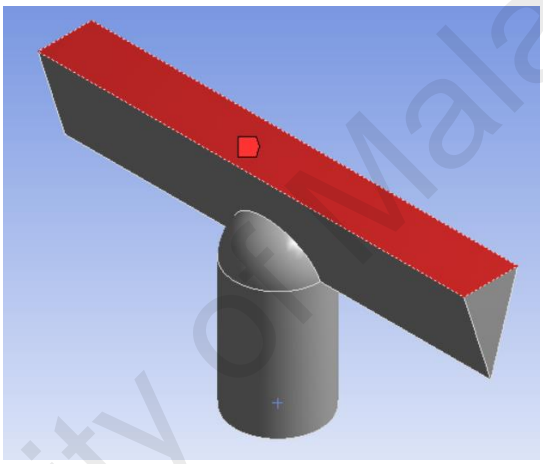

Figure 3.8:Outlet of the nozzle

3.5.1.2 Meshing of flat fan nozzle

The mesh method of the flat fan nozzle is the same as the combined flat fan nozzle.

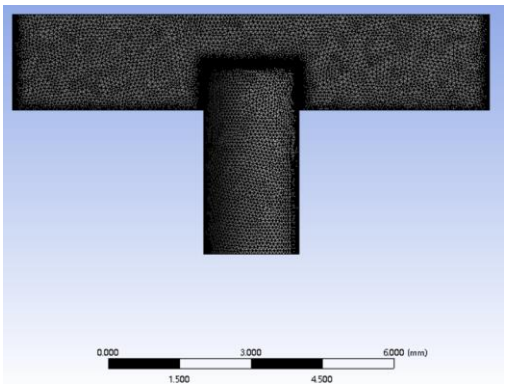

Figure 3.9: The front view of the mesh

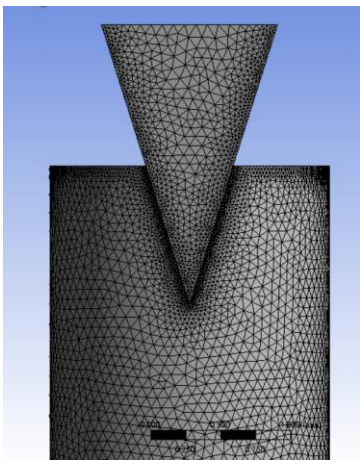

Figure 3.10: The left view of mesh

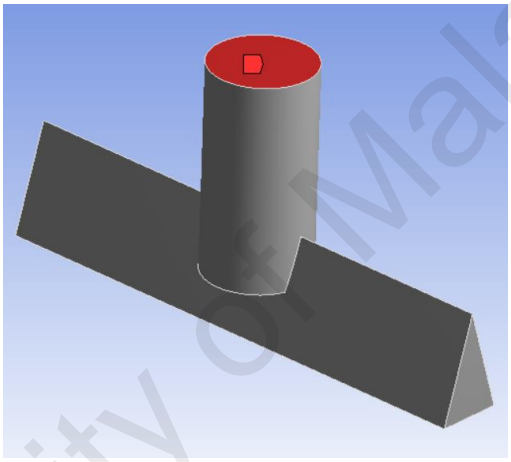

Figure 3.11:Inlet of nozzle

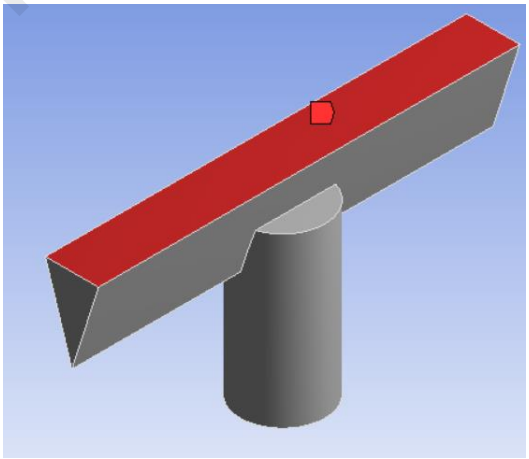

Figure 3.12:Outlet of nozzle

3.5.1.3 Mesh independence test

There is no huge difference in the structure and size of each fan nozzle. Select the combined nozzle with the parameter α=35°，D=2mm, L=3mm for mesh independence test. The mesh independence test can ensure that the number of mesh is sufficient and the accuracy of the simulation results. Generally, if the number of mesh elements increases, the accuracy of the contour of the model will also increase. Due to the version of ANSYS, the maximum number of mesh elements should be less than or equal to 512,000.

Table 3.2:Mesh independence results

Elements size(mm)	Mesh nodes	Mesh elements	Maximum pressure(pa)	Velocity of outlet(m/s)
0.095	101540	511449	288724.13	14.5771
0.1	99630	501161	288542.44	14.9805
0.15	90632	454690	289136.56	14.6311
0.2	89182	447260	289400.31	14.1558
0.25	88545	444395	289484.84	14.5760
0.3	88490	444185	289589.94	14.7165
0.4	88951	446675	289519.5	14.7039
0.5	88509	444233	289590.84	14.6373

The mesh element size is 0.095, the number of elements equal to 511449. When the number of elements bigger than 512000, the ANSYS not allowed to simulation. The element size of the fan nozzle model is between 0.08mm to 0.15mm and the number of elements is about 500,000.

3.5.2 Reynolds number

Reynolds number is used to judge the flow of fluid, and then predict the flow model. Under low Reynolds number, the fluid flows mainly in laminar flow, while under high

Reynolds number, fluid flow tends to be turbulent. The equation for calculating Reynolds number for flow in pipe as:

$$R_e = \frac{\rho u D_H}{\mu} = \frac{u D_H}{\nu} = \frac{Q D_H}{\nu A} = \frac{W D_H}{\mu A} \tag{8}$$

Where,D_H is hydraulic diameter of pipe, m; Q is the volume flow, m^3/s ; A is cross-sectional area of the pipe, m^2; u is the average velocity of fluid, m/s; μ is the dynamic viscosity of liquid, Pa·s; ν is the kinematic viscosity, m^2/s; ρ is liquid density,kg/m^3; W is the mass flow of liquid, kg/s.

Table 3.3: Reynolds number to judge flow characteristics

Reynolds number	less than 2300	Between 2300 and 4000	Greater than 4000
The flow in the pipeline	laminar	transient	turbulent

For the pressure inlet and outlet boundary conditions. FLUENT will calculate the inlet velocity of the fluid according to Bernoulli equation. The Bernoulli equation original expression as:

$$\frac{1}{2}\rho v^2 + \rho g h + p = constant \tag{9}$$

Where, v is liquid velocity, m/s; g is acceleration of gravity, m/s^2; h is the height where the fluid is located, m; p is the pressure at the chosen point, ; ρ is liquid density,kg/m^3. For incompressible liquids, when the fluid enters through the pressure inlet boundary, FLUENT uses the input boundary condition pressure as the total pressure of the fluid on the inlet plane to calculate the inlet velocity. The equation as:

$$p_0 = p_s + \frac{1}{2}\rho v^2 \quad (10)$$

Where, p_0 is the total pressure of the fluid on the inlet; p_s is the static pressure. The Y-velocity of initial value is calculated by FLUENT is 24.51697, m/s.

The u equals to 24.51697m/s, the density of water is 998.2, kg/ m^3 at 300K temperature. D_H equal to inlet diameter. The dynamic viscosity of water is 0.001003,$\frac{kg}{m} - s$. Because the initial inlet Y velocity of the nozzles are the same, and the Reynolds number is related to the inlet diameter of the nozzles. Therefore, the maximum(d=3mm) and minimum diameter(d=1mm) values were calculated into the equation 3.8.

$R_{e\,max} = 73198.9216 > 4000$

$R_{e\,min} = 24399.64 > 4000$

Therefore, the internal fluid of all nozzles is in turbulent flow.

3.5.3 Boundary Conditions

The setup options use double precision and solver processes are 8. Double precision requires longer calculation time than single precision, but the calculation result is more accurate than single precision. This simulation does not consider time, the purpose is to obtain complete simulation results. The Y-axis gravity acceleration set 9.81m/s^2. Solver options the type is selected pressure-based, velocity formulation is absolute, and the time is steady.

Water-liquid is added as a fluid material. Water-liquid is an incompressible liquid. The density of water-liquid is 998.2 kg/m^3 ,and the dynamic viscosity is 0.001003 kg/m-s at the temperature of 300 k. Set the cell zone conditions to water-liquid. The viscous model is chosen standard k-ε model. The boundary condition is selected pressure-inlet

and pressure-outlet. The inlet pressure are 300000 pascals cause the working pressure of the diaphragm pump are 300000 pascals, and the outlet pressure is standard atmospheric pressure that are 101325 pascals. In the boundary condition setting, the value of the fluid turbulence parameter needs to be set. The turbulence intensity and hydraulic diameter are selected to define the turbulence parameters (Jiang Fan, 2008). A turbulence intensity less than or equal to 5% is generally regarded as low-intensity turbulence, and a turbulence intensity greater than 10% is regarded as high-intensity turbulence. The turbulence intensity here is set to 5%, because the fan nozzle used for work is low-intensity turbulence. The definition and calculation formula of hydraulic diameter D_i as follow:

$$D_i = \frac{4A}{p} \tag{11}$$

Where, A is area section of the duct or pipe, p is wetted perimeter of the duct or pipe. The hydraulic is equal to cavity diameter. Solution methods is selected simple. Gradient is least squares cell based, cause the mesh is unstructured. Spatial discretization used standard pressure. The momentum, turbulent kinetic energy and turbulent dissipation rate are selected first order upwind. The first order is easier to converge than the second order, and the calculation time is shorter. The precision of the two is not much different, so first order is selected. The initialization methods chosen standard initialization and computed from inlet. The reference frame is absolute. For the pressure inlet, the flow direction and the specification of the total pressure are determined by the velocity formula. Because the previous velocity formula is an absolute formulation, it is also absolute here. The run calculation set the number of iterations is 400.

3.5.4 Turbulence models

Turbulence modeling is used to predict the effects of turbulence. It is used for mathematical model construction. The reason for many scales of eddy flow and strong

nonlinearity exists in turbulence makes the turbulence problem difficult to solve in theoretical experiments and numerical simulations. Navier - stokes equation can accurately describe the turbulent motion, but a lot of time is needed to solve such a complex equation. It is necessary to use the turbulence model to solve difficult turbulence problems.

3.5.4.1 Types of turbulence models

According to the number of partial differential equations in turbulence model can be classified. Commonly used turbulence models are: 1 equation model (Spalart-Allmaras), 2 equation model (κ-Epsilon model and $k-\omega$ model), 4 equation model (transition SST), and 7 equation model (Reynolds stress model) (Hanjalic & Launder, 1972). The following is a brief introduction to the above models.

The Spalart-Allmaras model is generally used for aviation problems. It is mainly the calculation of wall-bounded flow. The Spalart-Allmaras model can only solve the turbulent viscous transport equation, it cannot solve the length scale of the thickness of the shear layer. It is not suitable for solving the flow problem with a large change in flow scale.

The k-epsilon model is the simplest completed turbulence model. It solves the variable of velocity and length. In FLUENT, the standard k-ε model has a wide range of applications and reasonable precision. Since it was proposed, it has become an important tool for engineering flow field calculations (Langtry R B, 2009).

The standard k-ω model mainly solves the problems of low Reynolds number, compressibility, and shear flow. The k-ω model predicts the propagation rate of free shear flows, such as mixed flows, flow around plates, flows around cylinders and radial jets, so it is suitable applied to wall-bound flows and free shear flows.

The SST k-ω model is similar to the standard k-ω model. But SST k-ω model adds a hybrid function, which is designed for the near-wall area. SST k-ω model has higher accuracy and credibility than the standard k-ω model in a wide range of flow fields.

The Reynolds stress model has an important role in the calculation of 3D turbulent flow field and can effectively calculate the anisotropic turbulent flow field.

3.5.4.2 $\boldsymbol{k-\varepsilon}$ models

The $\boldsymbol{k-\varepsilon}$ models are divided into standard $\boldsymbol{k-\varepsilon}$ model**,** RNG $\boldsymbol{k-\varepsilon}$ model and realizable $\boldsymbol{k-\varepsilon}$ model. The following is a brief introduction to the above models.

1. The standard $\boldsymbol{k-\varepsilon}$ model is a half-empirical formula, which is summarized from experimental phenomena. The turbulent kinetic energy transport equation of the $\boldsymbol{k-\varepsilon}$ model is derived through accurate equations. The dissipation rate equation is obtained through physical reasoning and mathematical simulation of similar prototype equations. It is suitable for the analysis of completely turbulent flow models with negligible effects of molecular viscosity.

2. The RNG $\boldsymbol{k-\varepsilon}$ model adds a factor to the $\boldsymbol{\varepsilon}$ equation. The turbulent vortex is added and the calculation accuracy in this area is improved. RNG theory provides a formula for calculating low Reynolds number flow viscosity.

3. The advantage of realizable $\boldsymbol{k-\varepsilon}$ model is more accurate to calculate the divergence ratio of the flat and cylindrical jets because it adds the dissipation rate equation. It has better accuracy in strong streamline bending, vortex, and rotation.

The standard $k-\varepsilon$ model can usually simulate the real situation of fluid flow and is especially suitable for calculating the flow of pipes and channels. The standard $k-\varepsilon$ model is widely used in all kinds of flow research because of its simplicity and high

calculation accuracy (Wilcox, 2008). The fluid flow inside the nozzle is turbulent with high Reynolds number, and there is no vortex and rotation. Therefore, the standard $k-\varepsilon$ model is adopted in this study.

In the standard $k-\varepsilon$ model, the turbulence kinetic energy (k) equation and the turbulence dissipation rate (ε) equation are solved to obtain the solutions of k and ε, then the values of k and ε are used to calculate the turbulence viscosity. Finally, the solution of the Reynolds stress is obtained by the Boussinesq assumption. $k-\varepsilon$ variant of approximation of eddy viscosity model equation as:

$$\mu_t = \frac{\rho C_u k^2}{\varepsilon} \tag{12}$$

Turbulent kinetic energy k and turbulent dissipation rate ε equations are respectively shown in the following equation:

$$\frac{\partial}{\partial t}(\rho k) + \frac{\partial}{\partial x_i}(\rho k u_i) = \frac{\partial}{\partial x_j}\left[\left(\mu + \frac{\mu_t}{\sigma_k}\right)\frac{\partial k}{\partial x_j}\right] + G_k - \rho\varepsilon \tag{13}$$

$$\frac{\partial}{\partial t}(\rho \varepsilon) + \frac{\partial}{\partial x_i}(\rho \varepsilon u_j) = \frac{\partial}{\partial x_j}\left[\left(\mu + \frac{\mu_t}{\sigma_\varepsilon}\right)\frac{\partial \varepsilon}{\partial x_j}\right] + C_{1\varepsilon}\frac{\varepsilon}{k}G_k - C_{2\varepsilon}\rho\frac{\varepsilon^2}{k} \tag{14}$$

where, ρ is the continuous phase density, kg/m^3 ; ε is the turbulent dissipation rate, m^2/s^3; k is the turbulent kinetic energy, m^2/s^2; μ is the dynamic viscosity,$pa \cdot s$; σ_k is the Prandtl number of turbulent kinetic energy; σ_ε is the Prandtl number of dissipation rate of turbulent kinetic energy; G_k is the turbulent kinetic energy caused by laminar velocity gradient,pa/s; $C_{1\varepsilon}, C_{2\varepsilon}$ is the empirical constant. The equation of G_k as:

$$G_k = \mu_t \frac{\partial \mu_i}{\partial x_j}\left(\frac{\partial \mu_i}{\partial x_j} + \frac{\partial \mu_j}{\partial x_i}\right) \tag{15}$$

The model constants are $C_{1\varepsilon}$=1.44, $C_{2\varepsilon} = 1.92$, $C_u = 0.09$, $\sigma_k = 1.0$, $\sigma_\varepsilon = 1.3$.

CHAPTER 4: RESULTS AND DISCUSSION

4.1 Analysis of fluid flow of combined flat fan nozzle

After 400 iterations of combined flat fan nozzles with different parameter structures under the same conditions, the internal pressure and velocity are calculated through fluid mechanics. After convergence, through the comparison of the simulation results, the XY plane and YZ plane in the location settings are added, and then the pressure and velocity contours of the XY plane and YZ plane are added.

4.2 Effect of design parameter on performance

4.2.1 Effect of grooving angle on velocity, pressure, and mass flow

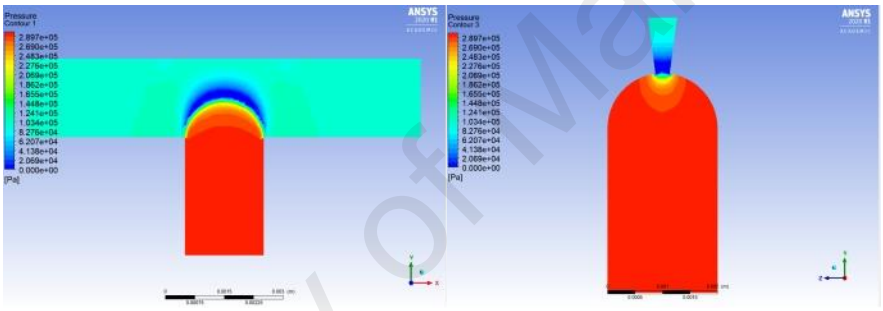

Figure 4.1: Pressure contours of XY section and YZ section of No.1 nozzle

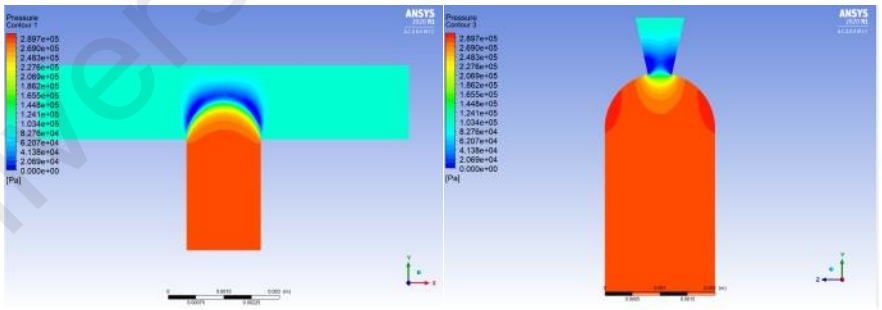

Figure 4.2: Pressure contours of XY section and YZ section of No.2 nozzle

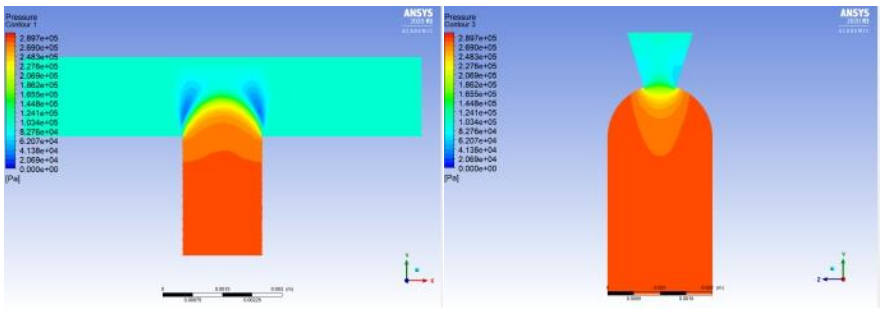

Figure 4.3: Pressure contours of XY section and YZ section of No.3 nozzle

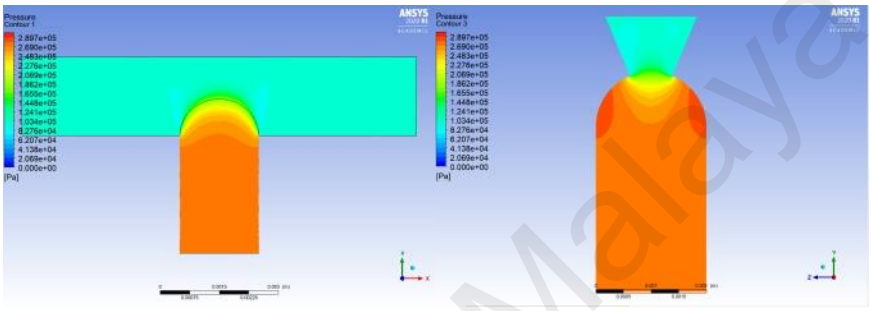

Figure 4.4: Pressure contours of XY section and YZ section of No.4 nozzle

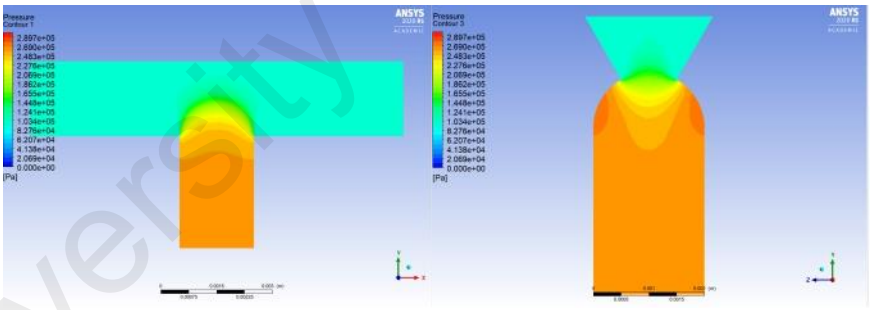

Figure 4.5: Pressure contours of XY section and YZ section of No.5 nozzle

The pressure range is set to user specified. The maximum pressure is 0.3Mpa and the minimum pressure is 0. In Figure 4.1 to Figure4.5, the red area shows that the pressure is 0.289Mpa; the orange area pressure is around 0.24Mpa; the yellow area pressure is around 0.22Mpa; the green area pressure is around 0.15Mpa; the blue area pressure is close to 0. From Figure4.1 can be seen the pressure is highest at the nozzle inlet, and the pressure at the nozzle outlet gradually decreases, reaching the minimum pressure value after leaving

the outlet. Then the pressure in the extension area of the nozzle is in the standard atmosphere (0.101Mpa). It means that the liquid has not reached the area. The pressure inside the throat is basically unchanged. With the increase of grooving angle, the pressure in the nozzle throat decreases. The pressure at the nozzle outlet is gradually decreasing. After the liquid leaves the outlet, the pressure disappears when it reaches the V-shaped wedge area.

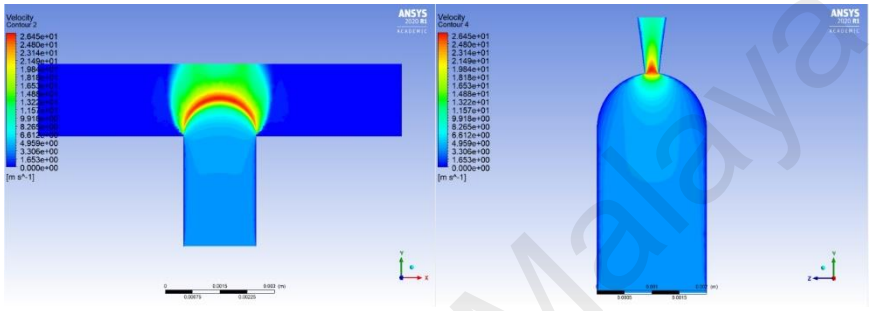

Figure 4.6: Velocity contours of XY section and YZ section of No.1 nozzle

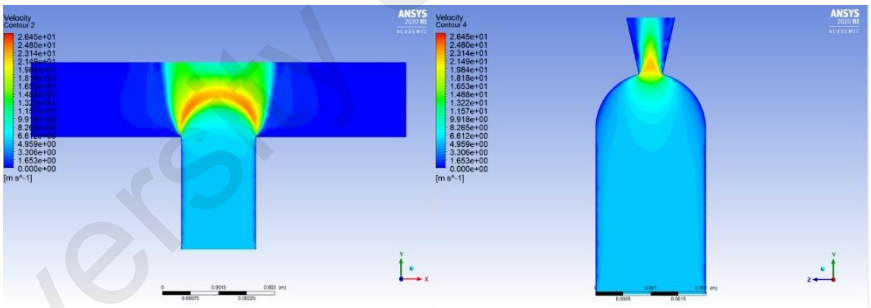

Figure 4.7: Velocity contours of XY section and YZ section of No.2 nozzle

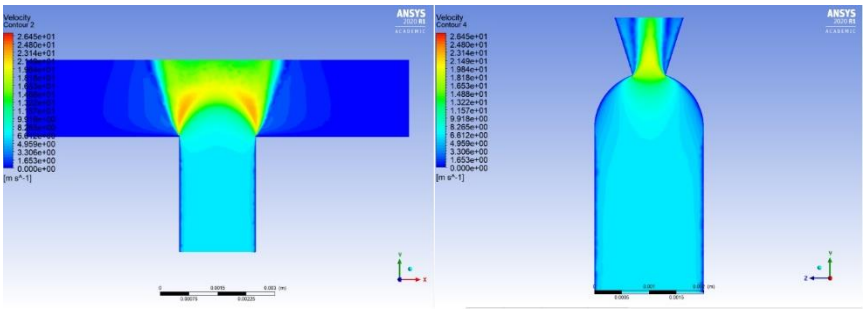

Figure 4.8: Velocity contours of XY section and YZ section of No.3 nozzle

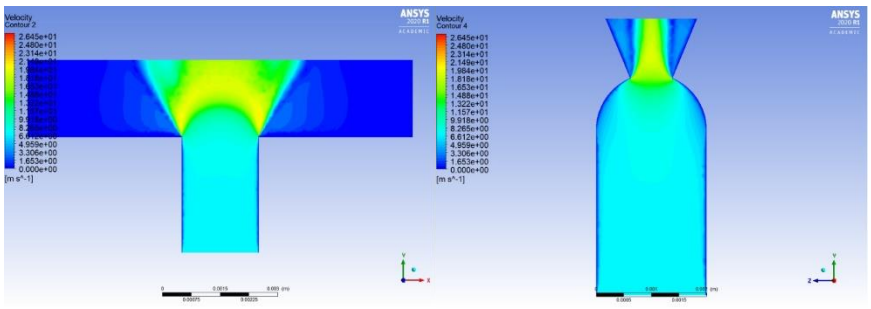

Figure 4.9: Velocity contours of XY section and YZ section of No.4 nozzle

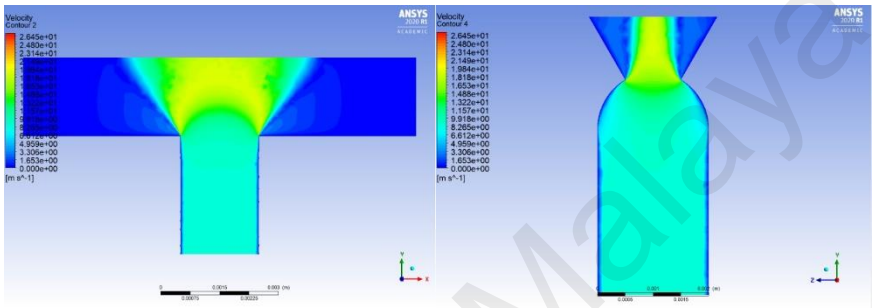

Figure 4.10: Velocity contours of XY section and YZ section of No.5 nozzle

The velocity range is set to user specified. The range of velocity is 0 m/s to 27 m/s. The red area velocity is around 26.5 m/s; the yellow area velocity is around 20 m/s; the green area velocity is around 15 m/s; the light blue area velocity is around 6 m/s; the blue area velocity is close to 0. From the Figure 4.6 to Figure 4.10 XY section, the velocity distribution of the fluid is fan shaped. When the velocity is small at the entrance of the nozzle, the velocity is the largest at the exit, and then gradually decreases. With the increase of grooving angle, the velocity in nozzle throat increases. The velocity at the nozzle outlet decreases with the increase of the grooving angle. Figure 4.6 to Figure 4.10 YZ section shows the liquid is sprayed from the outlet in a columnar shape. The maximum velocity appears around the outlet centerline. The greater the pressure, the smaller the velocity. And it can be seen from Figure 4.6 to Figure 4.10 XY section that the larger the grooving angle, the wider the angle at which the liquid is sprayed.

To compare the effect of the grooving angle more accurately on combined flat fan nozzle performance, ANSYS can draw the pressure and velocity data on the centerline of the nozzle into X-Y plots. It shows intuitive view of how the pressure and velocity are changing.

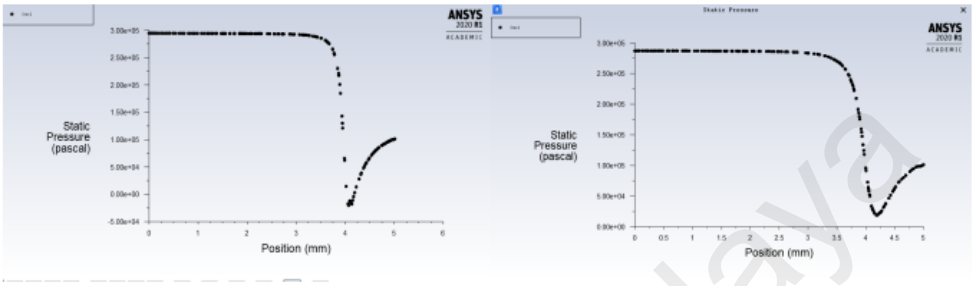

Pressure X-Y plots of No.1 nozzle

Pressure X-Y plots of No.2 nozzle

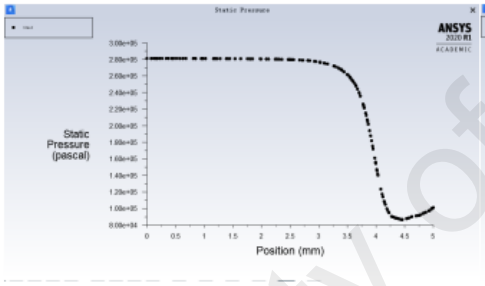

Pressure X-Y plots of No.3 nozzle

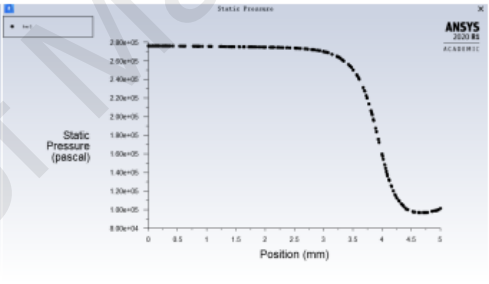

Pressure X-Y plots of No.4 nozzle

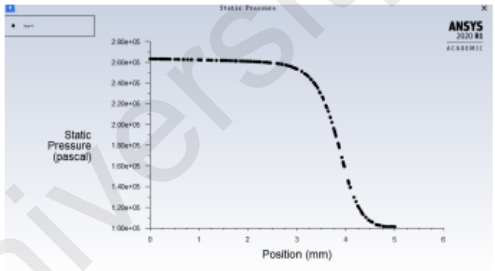

Pressure X-Y plots of No.5 nozzle

Figure 4.11: Pressure X-Y plots on the internal center line of nozzles with difference grooving angle

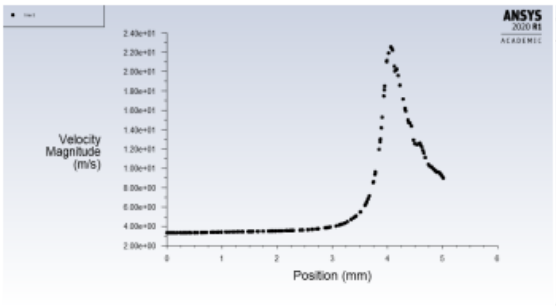

Velocity X-Y plots of No.1 nozzle

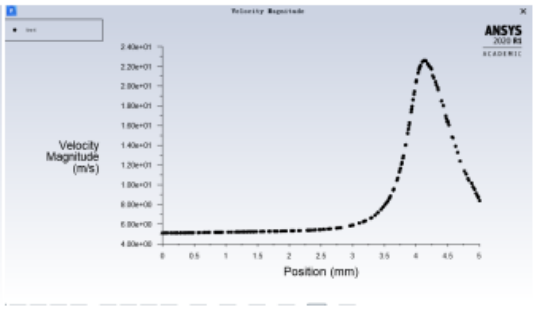

Velocity X-Y plots of No.2 nozzle

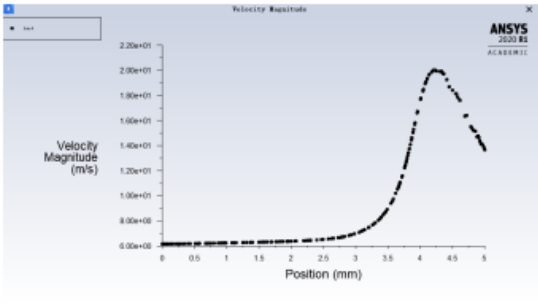

Velocity X-Y plots of No.3 nozzle

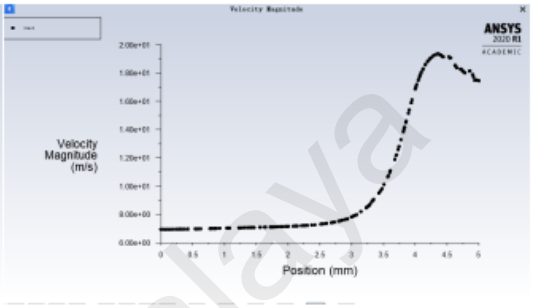

Velocity X-Y plots of No.4 nozzle

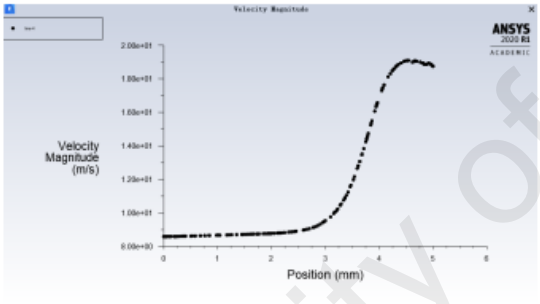

Velocity X-Y plots of No.5 nozzle

Figure 4.12: Velocity X-Y plots on the internal center line of nozzles with difference grooving angle

It can be seen from Figure 4.12 and 4.13 that the changing trend of the pressure and velocity of the liquid on the centerline of the nozzles. When the grooving angle is 15°, the velocity and pressure show the biggest change. When the grooving angle is equal to 60°, the pressure and velocity of the liquid on the nozzle centerline change more smoothly. After running the calculation, the report surface integrals are used to calculate the maximum pressure of the wall and the outlet maximum velocity of the Y-axis. The mass flow rate of inlet and outlet is calculated by fluxes.

Table 4.1:ANSYS calculated report of difference grooving angle nozzles

Nozzle No.	Inlet mass flow(kg/s)	Outlet mass flow(kg/s)	Mass flow net(kg/s)	Maximum pressure(pa)	Maximum velocity on centerline(m/s)
1	0.0011072983	-0.01107319	-2.077674e-07	295360.25	26.231766
2	0.015842517	-0.01584332	-8.120642e-07	291673.19	22.714499
3	0.019058417	-0.01905602	2.3933549e-06	288740.94	20.02075
4	0.021572373	-0.02157342	-1.04877e-06	284582.88	19.592033
5	0.026656134	-0.02665643	-3.018003e-07	276577.88	19.227665

It can be seen from Table 4.1 that the grooving angle has an influence on the mass flow. The greater the grooving angle of the fan nozzle, the greater the mass flow. To compare the results more intuitively, ANSYS is used to export the pressure and velocity on the centerline as a CSV file and make a graph. The pressure and velocity are placed on the centerline of the nozzle with the grooving angle of 15º, 25 º, 35 º, 45 º, 60 º in the same coordinate for comparison.

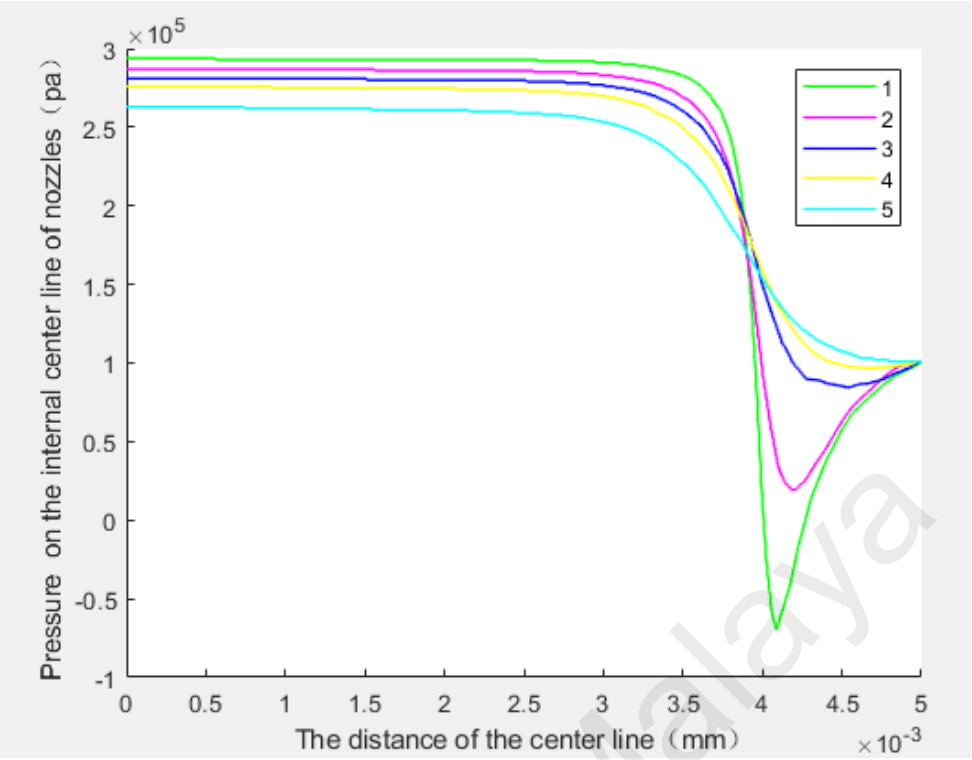

Figure 4.13: The center line fluid pressure curve of No.1, No.2, No.3, No.4, No.5 nozzles

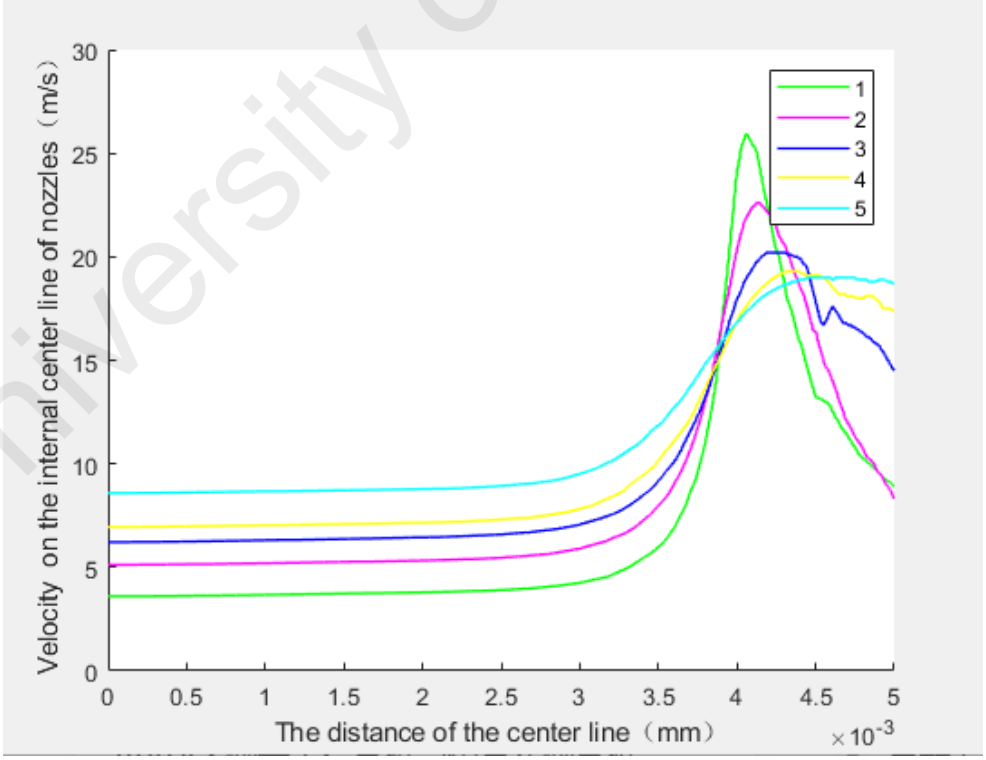

Figure 4.14: The center line fluid velocity curve of No.1, No.2, No.3, No.4, No.5 nozzles

Figure 4.13 and 4.14 intuitively shows the effect of changing the grooving angle of the nozzle on the velocity and pressure on the centerline of the nozzle under the condition of the same cavity diameter and length. The velocity changes greatly when the grooving angle is 15°-35°, but when the groove angle is 35°-60°, the velocity change is small. When the grooving angle is 15°, negative pressure occurs, which means that when the grooving angle is too small, the internal pressure of the nozzle is unstable. When the grooving angle is small, the pressure of the liquid in the nozzle is great. When the grooving angle is larger, the pressure of the liquid in the nozzle changes smoothly. The fluid velocity at the nozzle outlet is inversely proportional to the size of the grooving angle. That is the larger the slot angle of the nozzle, the slower the liquid velocity. The size of the grooving angle also influences the spray range. The larger the grooving angle, the wider the spray range. However, when the grooving angle is too large, the spraying velocity will decrease, and the spraying range will increase. Taking into account the problem of droplet deviation caused by the airflow generated by the wings of the drone when the drone is working and the flight speed of the agricultural drone, the maximum spray velocity should be greater than 20m/s. If the grooving angle is too large, uneven spraying and droplet drift will have occurred. If the grooving angle is too small, the pesticide spraying range is small, and the pesticide is concentrated in the center of the nozzle. Therefore, the appropriate grooving angle is 35°.

4.2.2 Effect of cavity diameter on velocity, pressure and mass flow

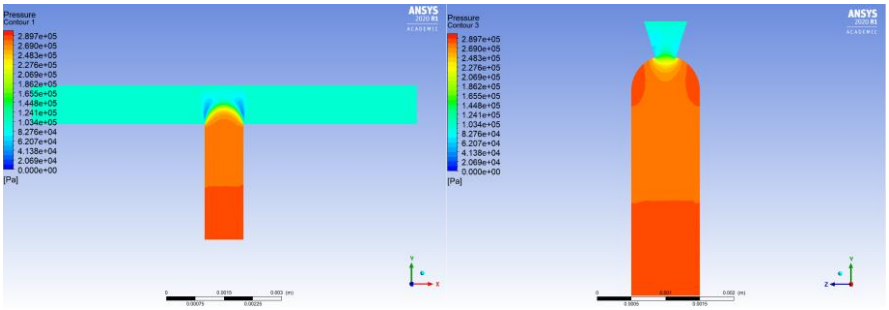

Figure 4.15: Pressure contours of XY section and YZ section of No.6 nozzle

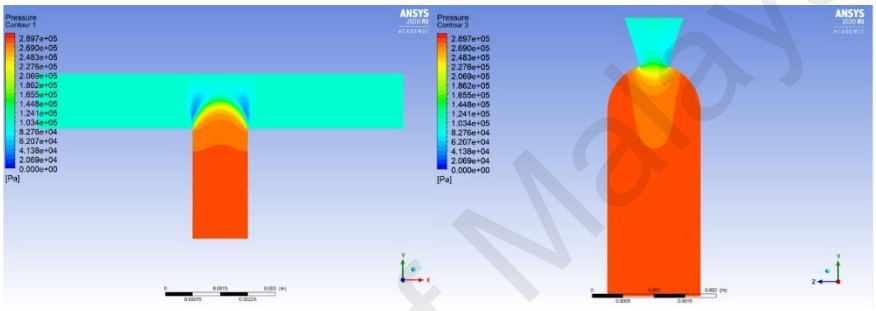

Figure 4.16: Pressure contours of XY section and YZ section of No.7 nozzle

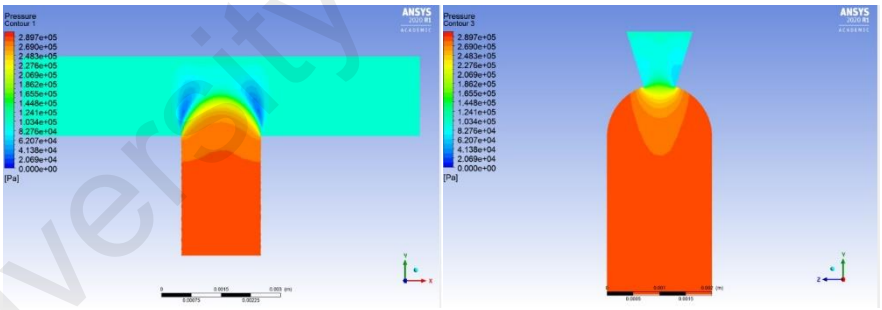

Figure 4.17: Pressure contours of XY section and YZ section of No.3 nozzle

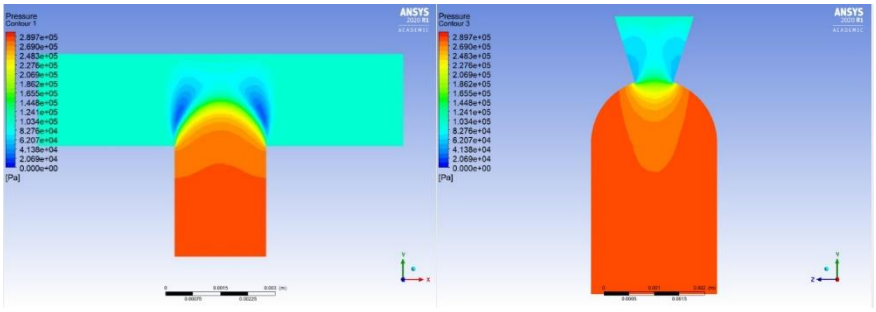

Figure 4.18: Pressure contours of XY section and YZ section of No.8 nozzle

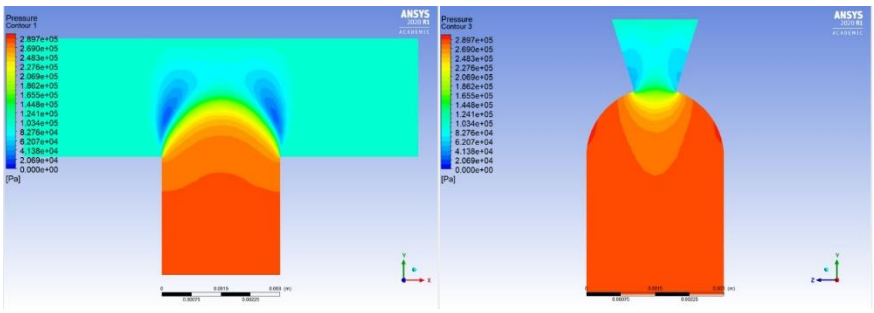

Figure 4.19: Pressure contours of XY section and YZ section of No.9 nozzle

The pressure range is set to user specified. The maximum pressure is 0.3Mpa and the minimum pressure is 0. In the Figure 4.15 to 4.19, the red area shows that the pressure is 0.289Mpa; the orange area pressure is around 0.24Mpa; the yellow area pressure is around 0.22Mpa; the green area pressure is around 0.15Mpa; the light blue area is around 0.07Mpa; the blue area pressure is close to 0. It can be seen the overall pressure distribution is also the same as Figure 4.1. The pressure is the largest in the throat, the pressure gradually decreases near the outlet, and the pressure reaches the minimum after leaving the nozzle.

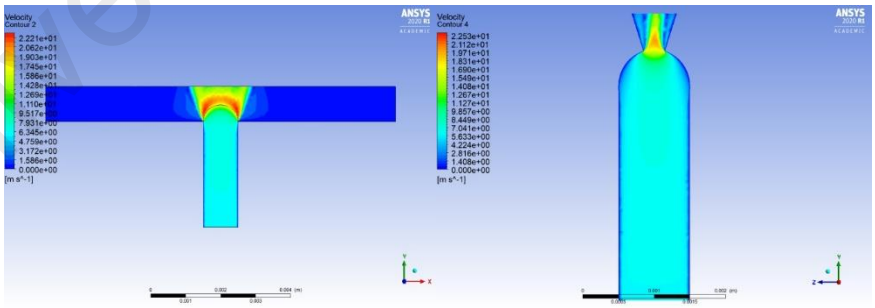

Figure 4.20: Velocity contours of XY section and YZ section of No.6 nozzle

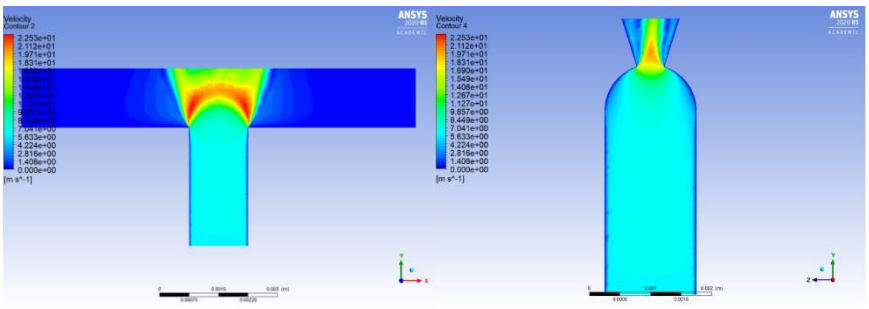

Figure 4.21: Velocity contours of XY section and YZ section of No.7 nozzle

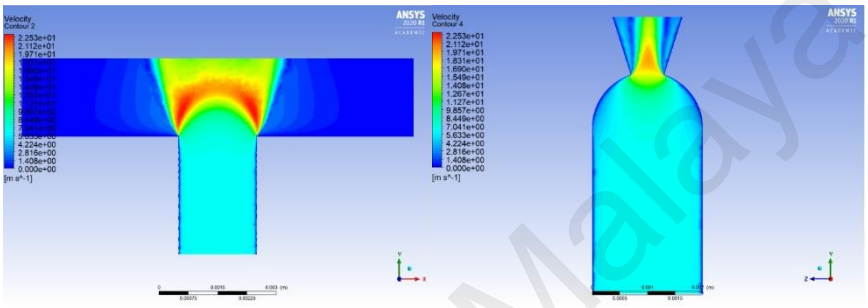

Figure 4.22: Velocity contours of XY section and YZ section of No.3 nozzle

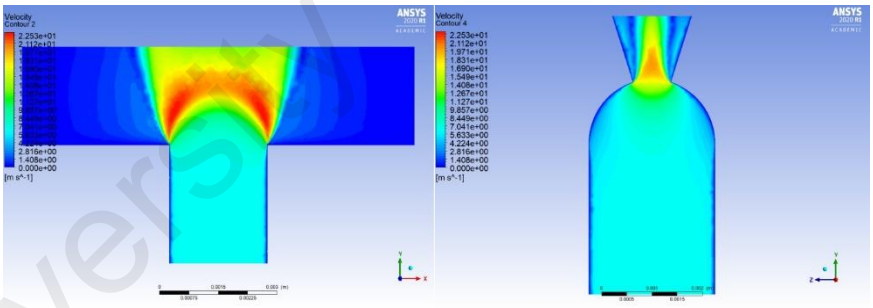

Figure 4.23: Velocity contours of XY section and YZ section of No.8 nozzle

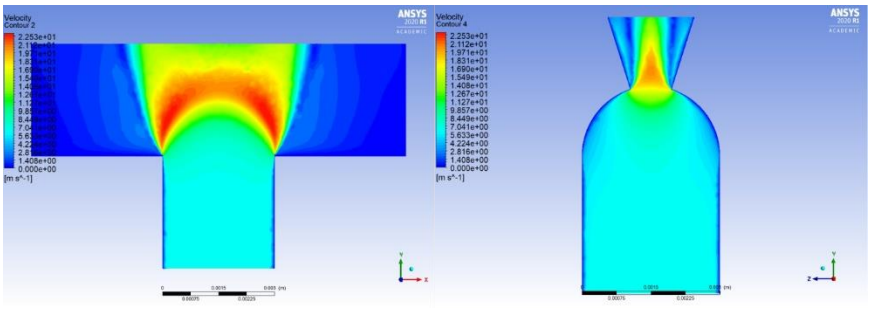

Figure 4.24: Velocity contours of XY section and YZ section of No.9 nozzle

The velocity range is set to user specified. The range of velocity is 0 m/s to 23 m/s. The red area velocity is around 22.2 m/s; the yellow area velocity is around 17 m/s; the green area velocity is around 13 m/s; the light blue area velocity is around 6 m/s; the blue area velocity is close to 0. From Figure 4.20 to 4.24 can be seen the overall velocity distribution is almost the same as Figure 4.6. The difference is that when the diameter of the cavity is changed, the velocity in the throat does not change much. It shows that the diameter of the cavity has little effect on the velocity of the liquid in the nozzle. From the above Figures XY section can be seen the cavity diameter has no effect on the angle at which the liquid is sprayed.

To accurately compare the effect of cavity diameter on combined flat fan nozzle performance, the pressures, and velocities data on the centerline of the nozzle were drawn into X-Y plots. It shows an intuitive view of how the pressure and velocity are changing.

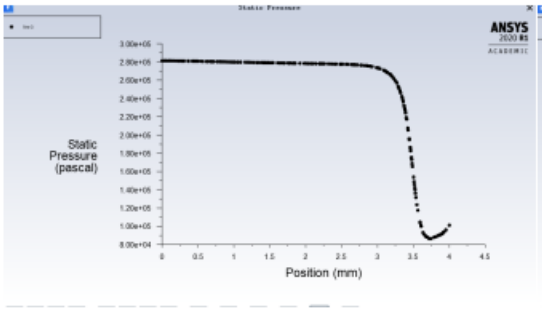

Pressure X-Y plots of No.6 nozzle

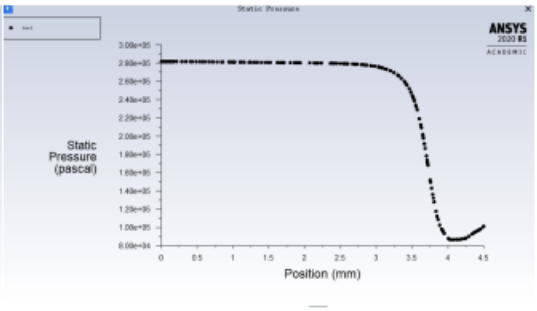

Pressure X-Y plots of No7. nozzle

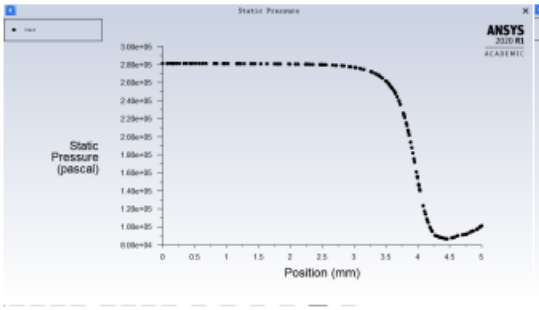

Pressure X-Y plots of No.3 nozzle

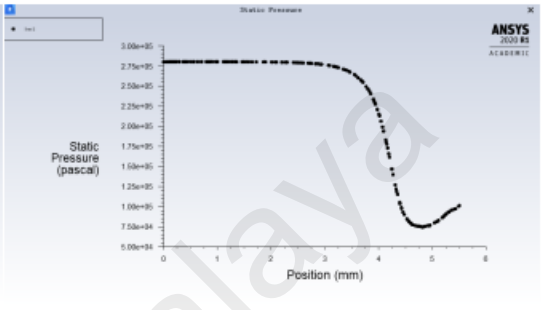

Pressure X-Y plots of No.8 nozzle

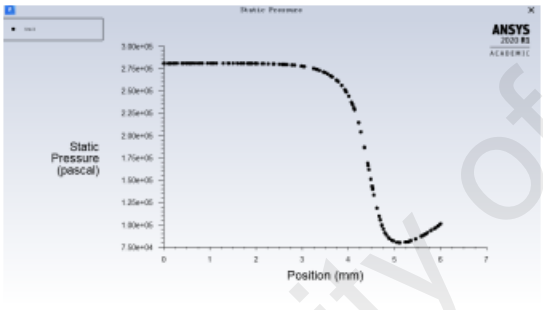

Pressure X-Y plots of No.9 nozzle

Figure 4.25: Pressure X-Y plots on the internal center line of nozzles with difference cavity diameter

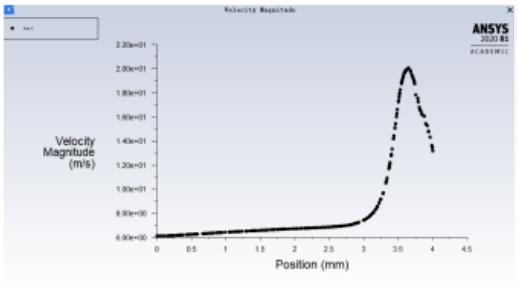

Velocity X-Y plots of No.6 nozzle

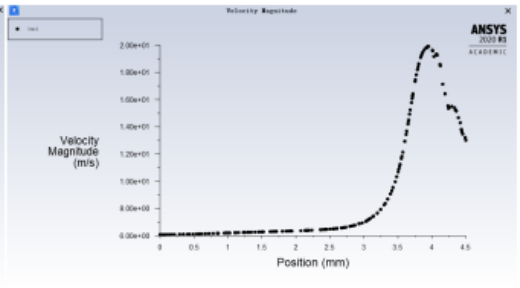

Velocity X-Y plots of No.7 nozzle

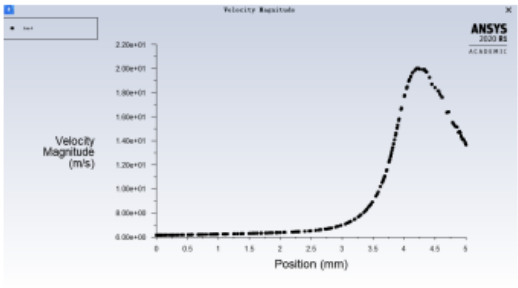

Velocity X-Y plots of No.3 nozzle

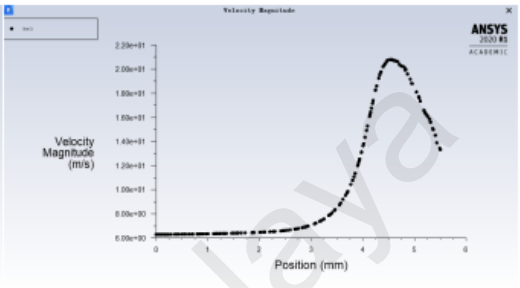

Velocity X-Y plots of No.8 nozzle

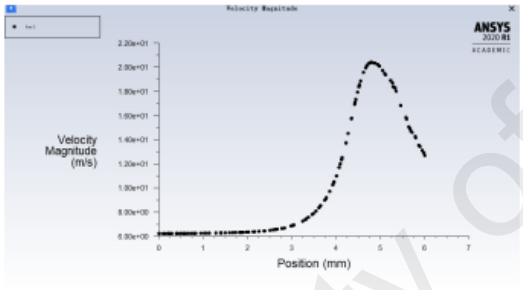

Velocity X-Y plots of No.9 nozzle

Figure 4.26: Velocity X-Y plots on the internal center line of nozzles with difference cavity diameter

After running the calculation, the report surface integrals are used to calculate the maximum pressure and the outlet maximum velocity of the Y-axis. The mass flow rate of inlet and outlet is calculated by fluxes.

Table 4.2: ANSYS calculated report of difference cavity diameter nozzles

Nozzle No.	Inlet mass flow （kg/s）	Outlet mass flow（kg/s）	Mass flow net （kg/s）	Maximum pressure(pa)	Maximum velocity on centerline(m/s)
6	0.0047026896	-0.0047023486	3.4092671 e-07	284501.53	20.228914
7	0.010629301	-0.010629037	2.6390126 e-07	287291.38	20.067152
3	0.019058417	-0.019056024	2.3933549 e-06	288740.94	20.02075
8	0.030047152	-0.030038229	8.9233028 e-06	290000.25	20.381876
9	0.043789724	-0.043778536	1.1187573 e-05	290573.34	20.630926

It can be seen from Table 4.2 that the cavity diameter has an influence on the mass flow. The larger the diameter of the cavity of the fan nozzle, the larger the mass flow. The maximum velocity is 20.63 m/s when the cavity diameter is 3 mm. The minimum velocity is 20.02 m/s when the cavity diameter equals to 2mm. To compare the results more intuitively, used ANSYS to export the pressure and velocity on the centerline as a CSV file, and make a graph. The pressure and velocity are put on the centerline of the nozzle with the cavity diameters of 1mm, 1.5mm, 2mm, 2.5mm, 3mm in the same coordinate system for comparison.

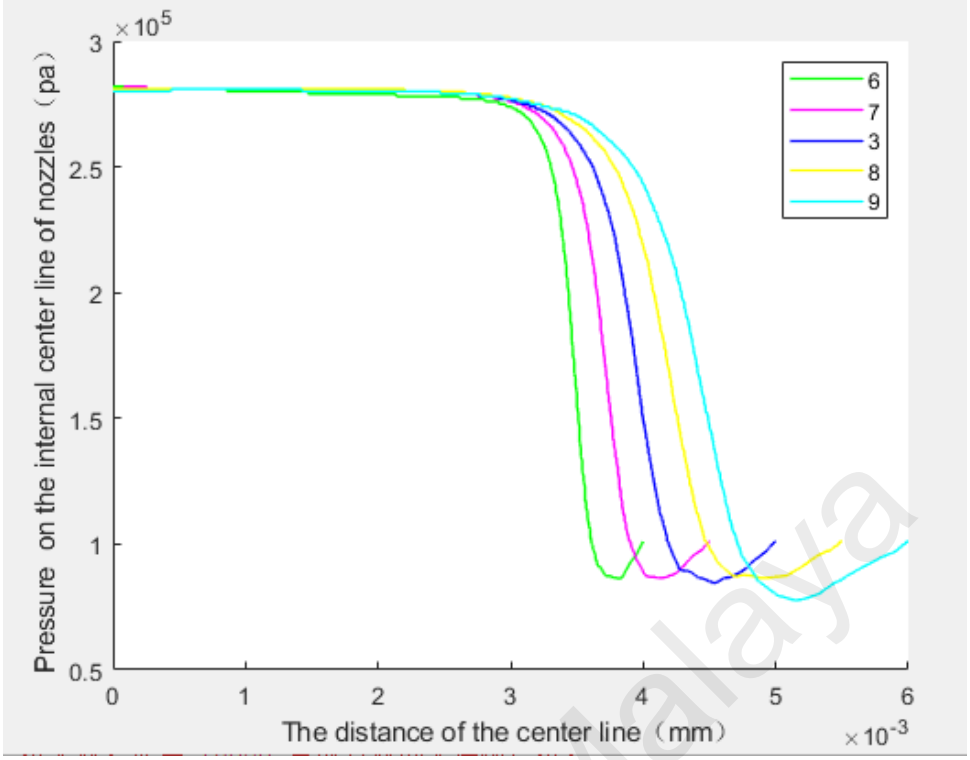

Figure 4.27: The center line fluid pressure curve of No.6, No.7, No.3, No.8, No.9 nozzles

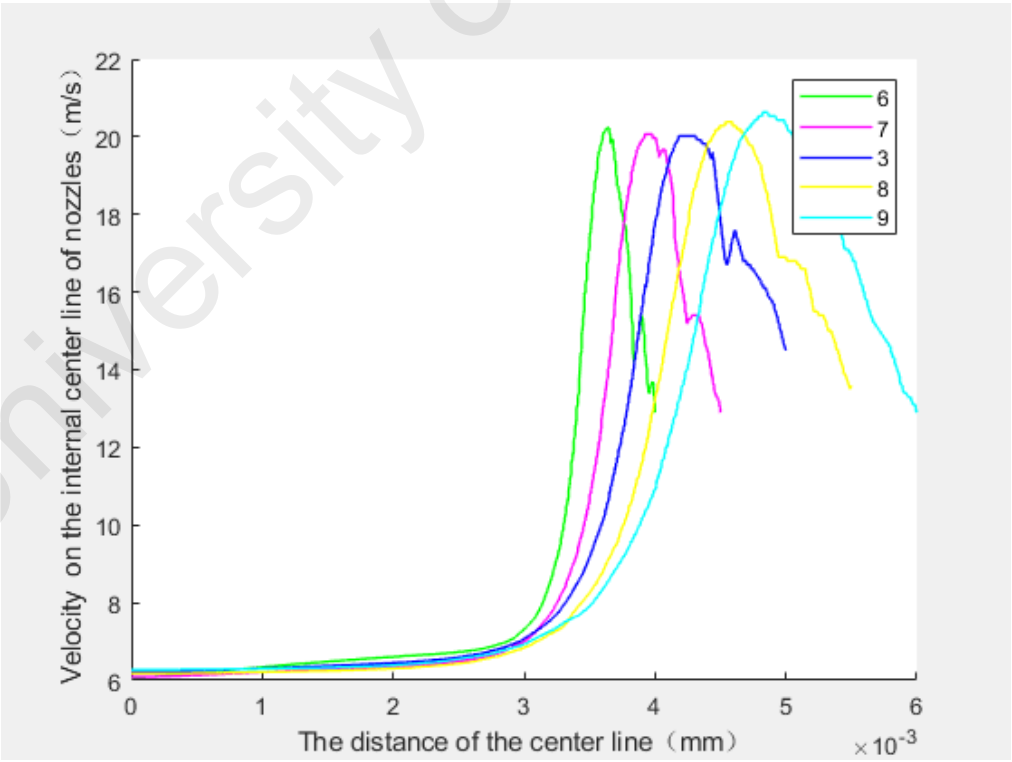

Figure 4.28: The center line fluid velocity curve of No.6, No.7, No.3, No.8, No.9 nozzles

Since the cavity diameter of the combined flat fan nozzle changed, the radius of the head of the nozzle also changes accordingly. Therefore, the total length of each nozzle is different. Figure 4.28 shows that the initial pressure value of each nozzle at the centerline is the same, then gradually decreases and then increases after leaving the outlet. When the cavity diameter is 3 mm, the outlet pressure is the smallest. Figure 4.29 shows that the initial velocity value of each nozzle at the centerline is the same, then gradually increases and then decreases after leaving the outlet. From the result data, it is concluded that the nozzle with the best performance is with a cavity diameter equal to 3 mm.

4.2.3 Effect of throat length on velocity, pressure and mass flow

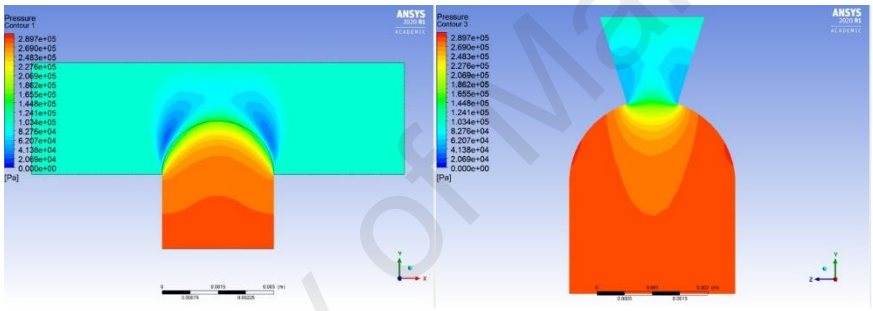

Figure 4.29: Pressure contours of XY section and YZ section of No.10 nozzle

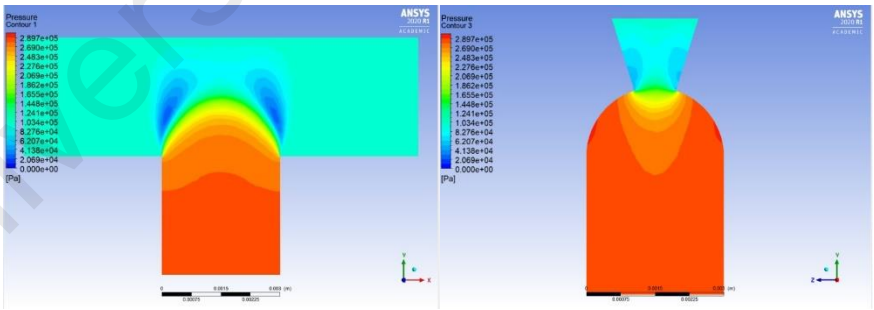

Figure 4.30: Pressure contours of XY section and YZ section of No.9 nozzle

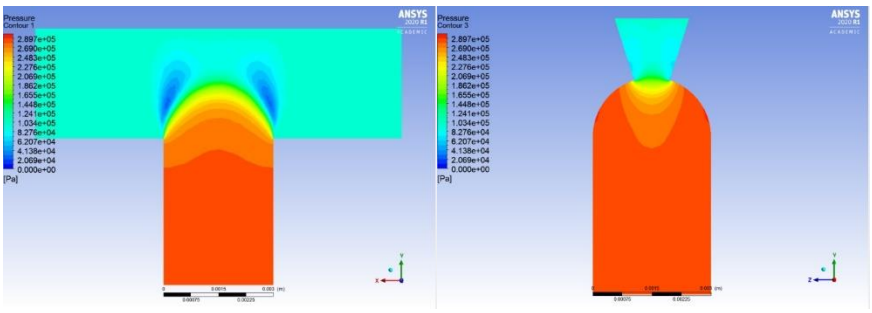

Figure 4.31: Pressure contours of XY section and YZ section of No.11 nozzle

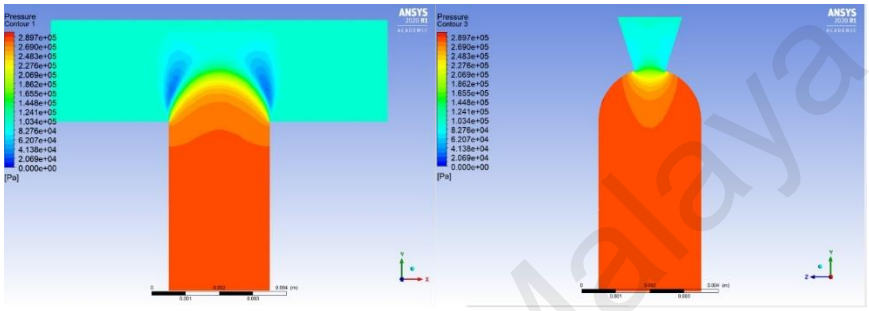

Figure 4.32: Pressure contours of XY section and YZ section of No.12 nozzle

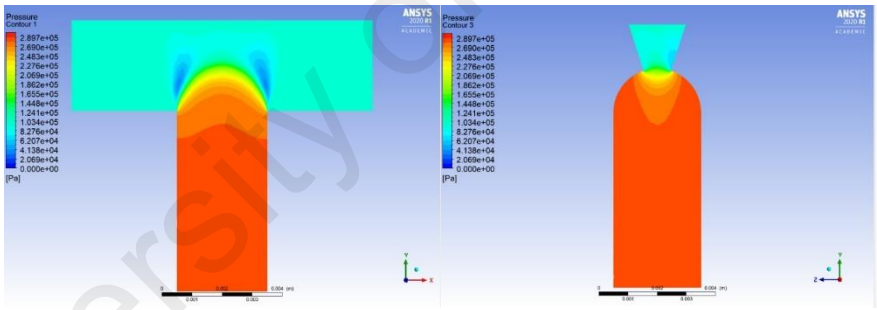

Figure 4.33: Pressure contours of XY section and YZ section of No.13 nozzle

The pressure range is set to user specified. The maximum pressure is 0.3Mpa and the minimum pressure is 0. In the Figure 4.29 to 4.33, the red area shows that the pressure is 0.289Mpa; the orange area pressure is around 0.24Mpa; the yellow area pressure is around 0.22Mpa; the green area pressure is around 0.15Mpa; the light blue area is around 0.07Mpa; the blue area pressure is close to 0. It can be seen from the above Figures the overall pressure distribution is also the same as the previous nozzle. The pressure is the

largest in the throat, the pressure gradually decreases near the outlet, and the pressure reaches the minimum after leaving the nozzle.

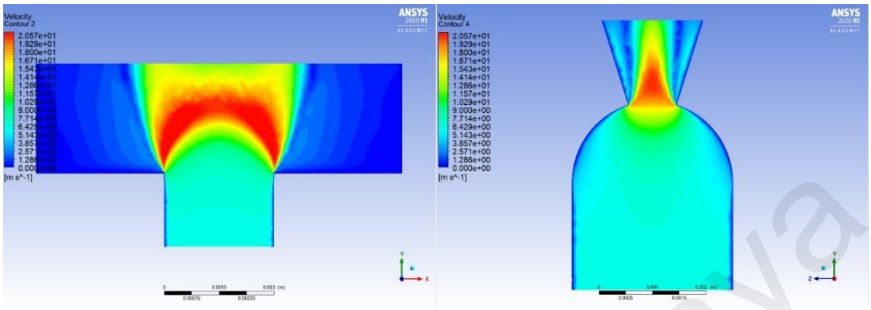

Figure 4.34: Velocity contours of XY section and YZ section of No.10 nozzle

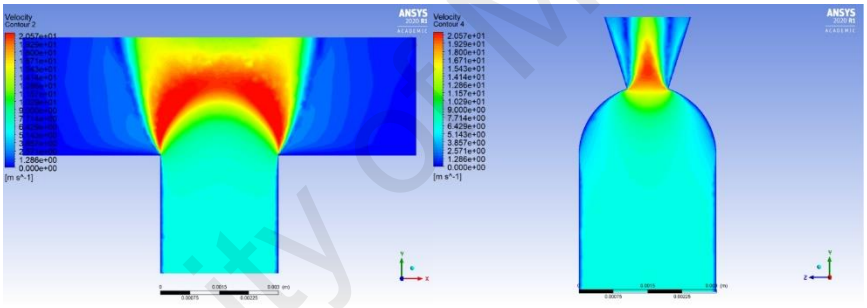

Figure 4.35: Velocity contours of XY section and YZ section of No.9 nozzle

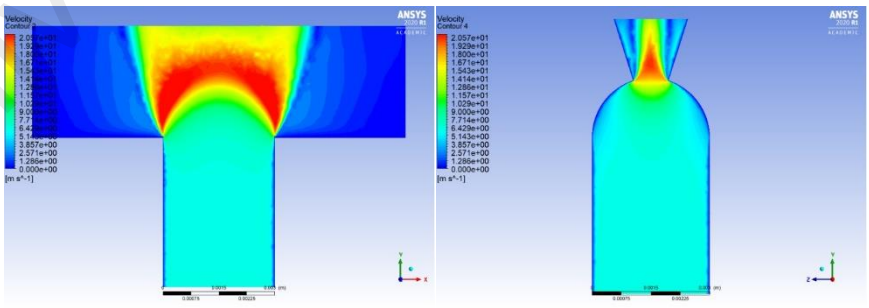

Figure 4.36: Velocity contours of XY section and YZ section of No.11 nozzle

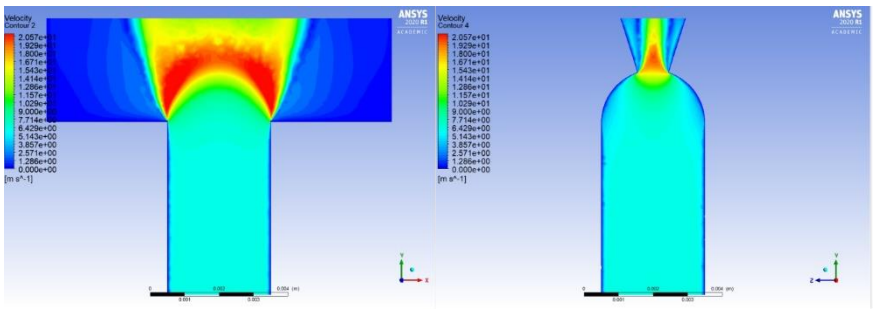

Figure 4.37: Velocity contours of XY section and YZ section of No.12 nozzle

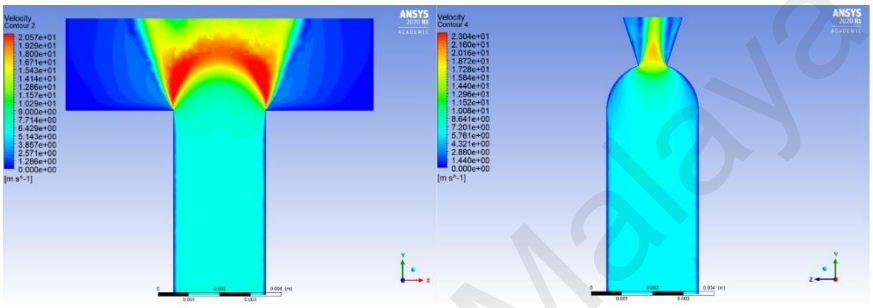

Figure 4.38: Velocity contours of XY section and YZ section of No.13 nozzle

The velocity range is set to user specified. The range of velocity is 0 m/s to 21 m/s. The red area velocity is around 20.5 m/s; the yellow area velocity is around 16 m/s; the green area velocity is around 10 m/s; the light blue area velocity is around 5.5 m/s; the blue area velocity is close to 0. From the above Figures can be seen the overall velocity distribution is almost the same as previous nozzle. From Figure 4.34 to 4.38 YZ section it can be seen the red area is decreases with the length increase. This means that the nozzle length affects the maximum outlet velocity. From Figure 4.34 to 4.38 XY section it can be seen the throat length has no effect on the angle at which the liquid is sprayed.

To compare the effect of throat length more accurately on combined flat fan nozzle performance, ANSYS is used to draw the pressure and velocity data on the centerline of the nozzle into X-Y plots. It shows an intuitive view of how the pressure and velocity are changing.

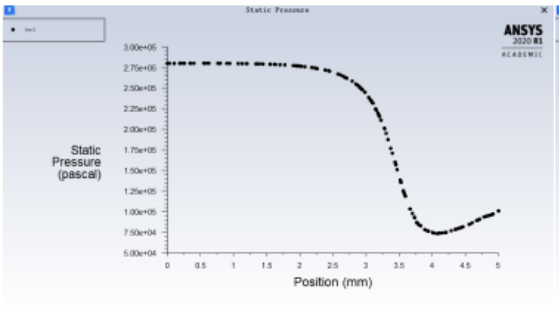

Pressure X-Y plots of No.10 nozzle

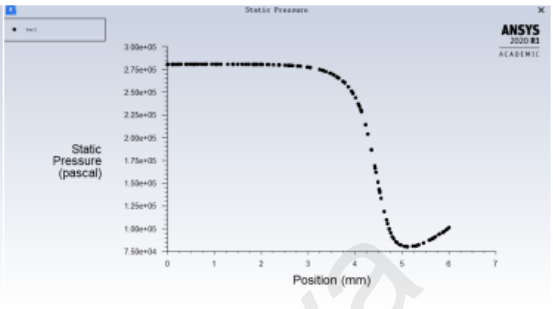

Pressure X-Y plots of No.9 nozzle

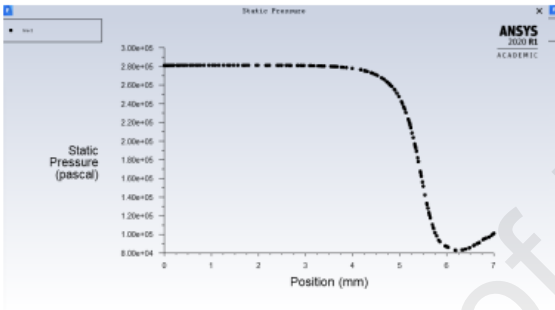

Pressure X-Y plots of No.11 nozzle

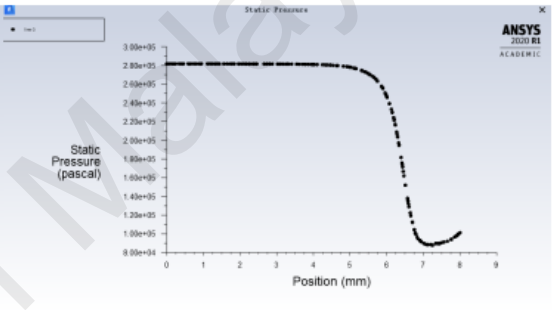

Pressure X-Y plots of No.12 nozzle

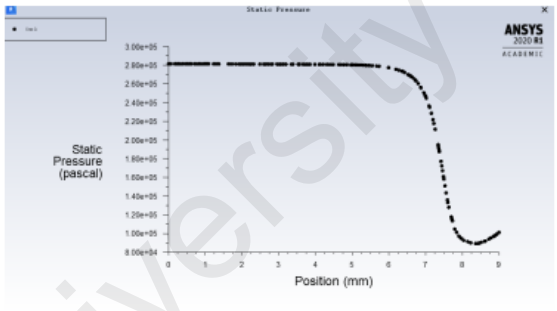

Pressure X-Y plots of No.13 nozzle

Figure 4.39 Pressure X-Y plots on the internal center line of nozzles with difference throat length

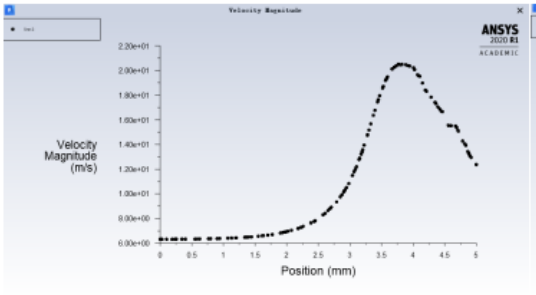

Velocity X-Y plots of No.10 nozzle

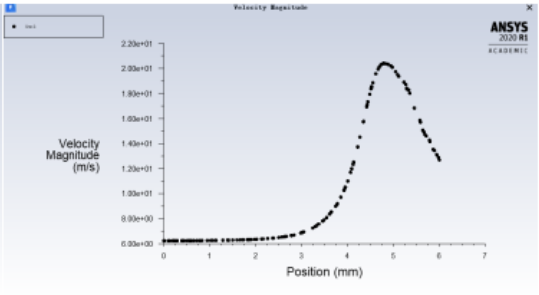

Velocity X-Y plots of No.9 nozzle

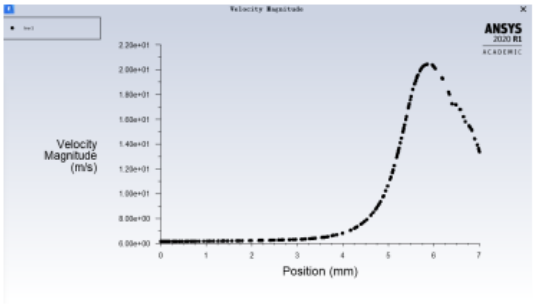

Velocity X-Y plots of No.11 nozzle

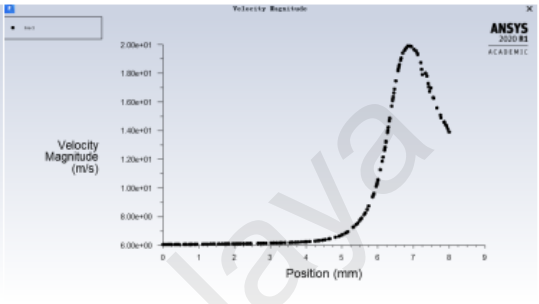

Velocity X-Y plots of No.12 nozzle

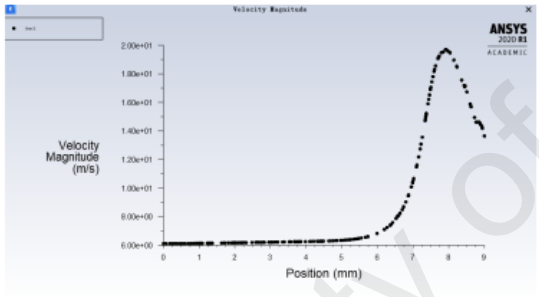

Velocity X-Y plots of No.13 nozzle

Figure 4.40: Velocity X-Y plots on the internal center line of nozzles with difference throat length

After running the calculation, the report surface integrals are used to calculate the maximum pressure of a liquid and the outlet maximum velocity of the Y-axis. The mass flow rate of inlet and outlet is calculated by fluxes.

Table 4.3: ANSYS calculated report of difference throat length nozzles

Modeling	Inlet mass flow（kg/s）	Outlet mass flow（kg/s）	Mass flow net（kg/s）	Maximum pressure(pa)	Maximum velocity on centerline(m/s)
α35D3L2	0.044293605	-0.044283782	9.82231e-06	290395.97	20.70553
α35D3L3	0.043789724	-0.043778536	1.1187573e-05	290573.34	20.630926
α35D3L4	0.043251155	-0.043244774	6.3811239e-06	290673.47	20.632229
α35D3L5	0.042739813	-0.042733276	6.5370647e-06	290031.75	20.040216
α35D3L6	0.042896121	-0.042895604	5.1617668e-07	289618.31	19.795218

As can be seen from Table 4.3 that the length of the throat has a minimal effect on the mass flow. To further compare the changes of velocity and pressure in the internal flow field of nozzles with different lengths more clearly, the velocity and pressure are extracted data on the center line of the internal flow field of each nozzle, and select the curve chart shown in the following figure to describe it.

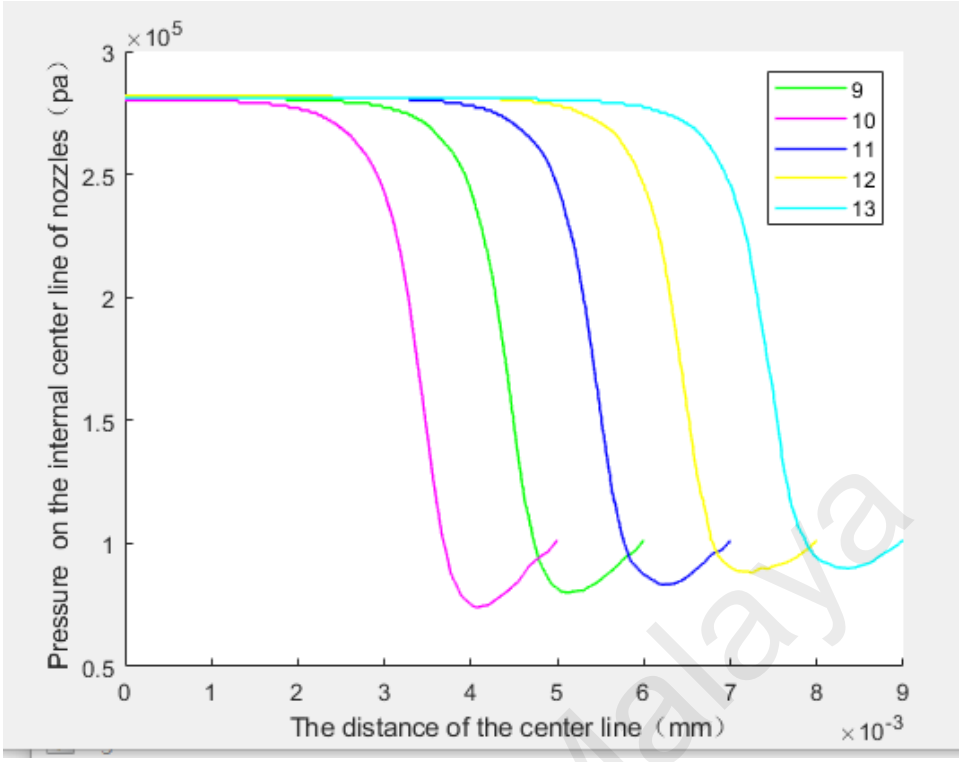

Figure 4.41: The center line fluid pressure curve of No.10, No.9, No.11, No.12, No.13 nozzles

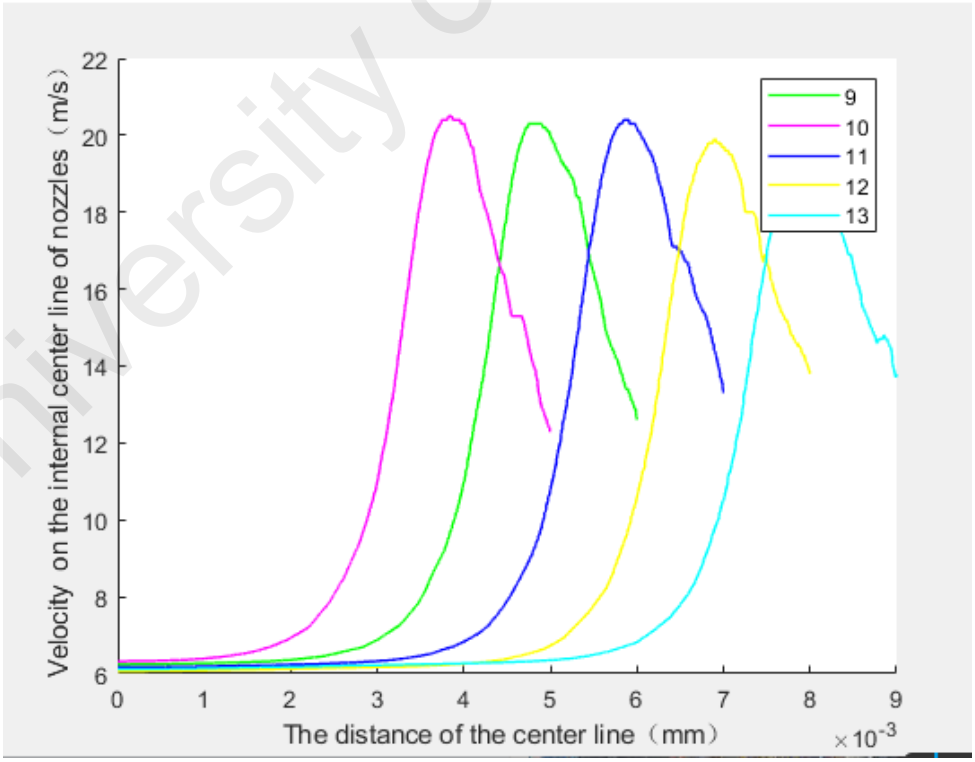

Figure 4.42: The center line fluid velocity curve of No.10, No.9, No.11, No.12, No.13 nozzles

It can be seen from Figure 4.42 that under the same condition that the combined flat fan nozzles keep the grooving angle and cavity diameter unchanged. As the length of the throat increases, the maximum pressure decreases. Figure 4.43 shows that the maximum velocity of the center line is related to the length of the throat. This is the length of the throat increases and the maximum velocity decreases. But the nozzle throat length has little effect on the maximum velocity. Therefore, the length of the throat to obtain the best performance is 2mm.

4.3 Compare the performance of flat fan and combined flat fan nozzles

Based on the above experimental data, the best nozzle parameters are summarized as the grooving angle equal to 35°, the cavity diameter equal to 3mm, the throat length equal to 2mm. To compare the performance difference between flat fan nozzles and combined flat fan nozzles, the α=35°, D=3mm, L=2mm flat nozzles are selected for simulation analysis under the same conditions.

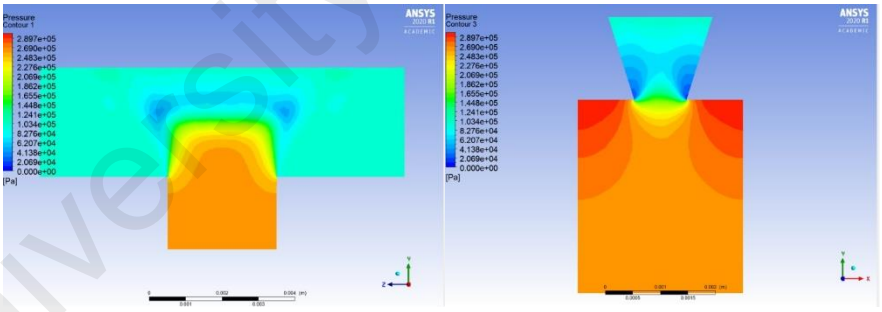

Figure 4.43: Pressure contours of XY section and YZ section of flat fan nozzle

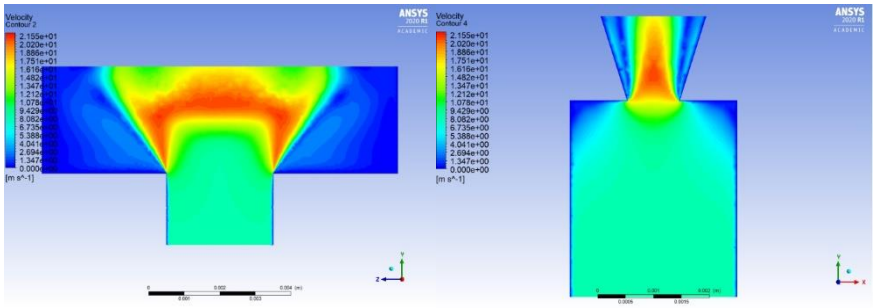

Figure 4.44: Velocity contours of XY section and YZ section of flat fan nozzle

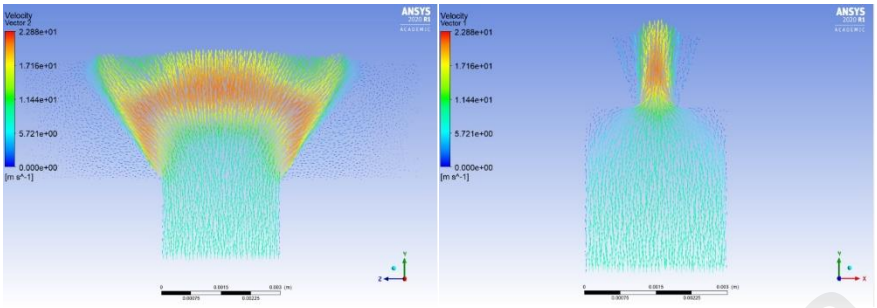

Figure 4.45: Velocity vector of XY section and YZ section of flat fan nozzle

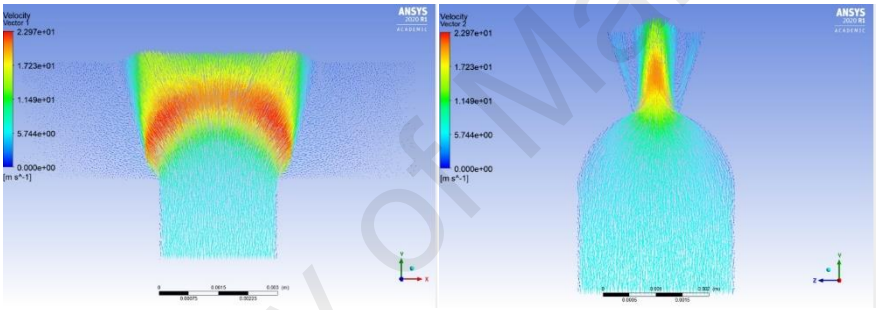

Figure 4.46: Velocity vector of XY section and YZ section of combined flat fan nozzle

The pressure range is set to user specified. The maximum pressure is 0.3Mpa and the minimum pressure is 0. In the Figure 4.19, the red area shows that the pressure is 0.289Mpa; the orange area pressure is around 0.25Mpa; the yellow area pressure is around 0.22Mpa; the green area pressure is around 0.15Mpa; the light blue area is around 0.08Mpa; the blue area pressure is close to 0. By comparing Figure 4.44 with the pressure contour of No.10 combined flat fan nozzle. The pressure inside the throat of the flat fan nozzle is lower than that of the combined flat fan nozzle. The flat nozzle has a lot of pressure at the edge of the outlet, because of the internal structure, the inside of the flat fan nozzle suffers a lot of pressure. The inner wall of the combined flat fan nozzle is spherical, the pressure can be smoothly led out of the nozzle, and the inside of the nozzle

will not suffer strong pressure. From Figure 4.45 the liquid sprayed by the flat fan nozzle is in the shape of the middle is higher and sides are lower. The spray shape of the combined flat fan nozzle shows an approximate normal curve distribution (Fan Rong, 2016). The flat fan nozzle spray velocity at the edge of the nozzle outlet is 0, and the spray performance is unstable. By comparing Figure 4.46 and Figure 4.47, it can be seen that the spray range of the flat fan nozzle is wider, but the spray distribution is uneven, and the droplets are sparse. The spray distribution of the combined fan nozzle is concentrated and evenly distributed.

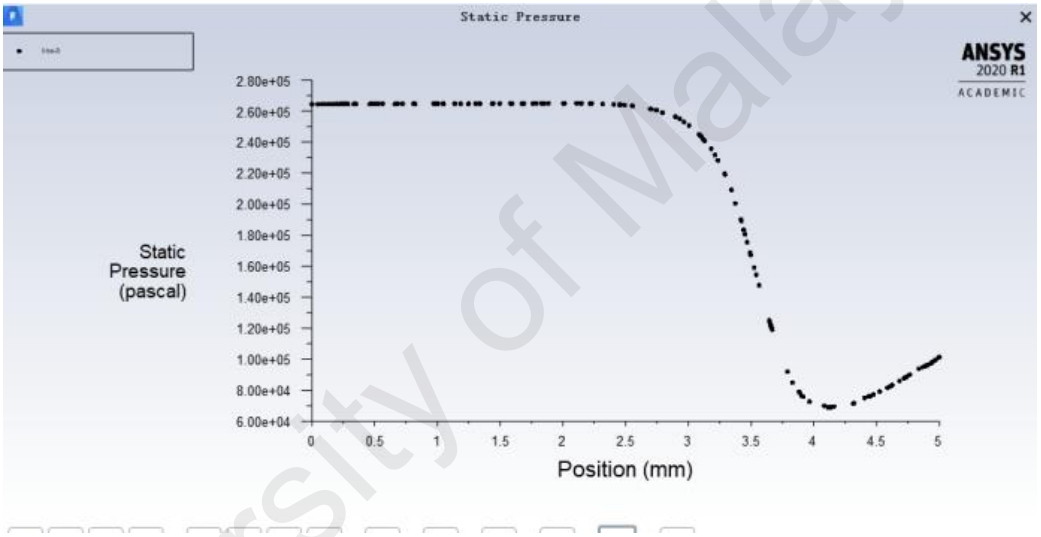

Figure 4.47: Pressure X-Y plots on the internal center line of flat fan nozzle

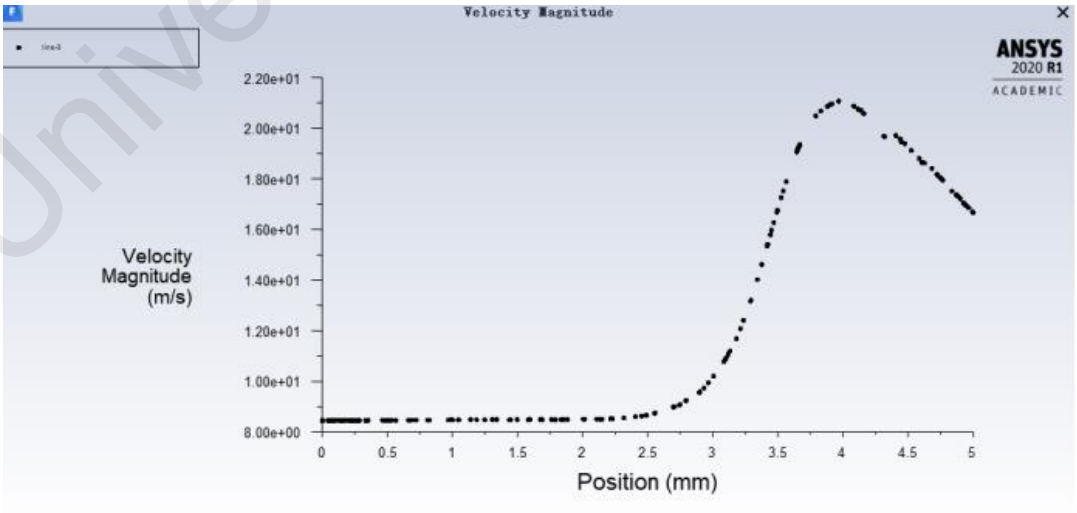

Figure 4.48:Velocity X-Y plots on the internal center line of flat fan nozzle

The pressure and velocity X-Y plots on the centerline are basically the same as combined flat fan nozzle No.10. The pressure arrived the largest at the inlet, the minimum pressure at the outlet, and then back again increases. The velocity is the smallest at the inlet, reaches the maximum at the outlet, and then decreases again. To compare the performance difference of the two nozzles, the pressure and velocity on the centerline are calculated by surface integrals and listed in a table.

Table 4.4: ANSYS calculated report of difference type nozzles

Modeling	Inlet mass flow(kg/s)	Outlet mass flow(kg/s)	Mass flow net(kg/s)	Maximum pressure(pa)	Maximum velocity on centerline(m/s)
Flat fan nozzle	0.059340979	-0.059350917	-9.9379098e-06	296485.5	21.185452
Combined flat fan nozzle	0.044293605	-0.044283782	9.82231e-06	290395.97	20.70553

It can be seen from Table 4.4 that the maximum pressure of the flat fan nozzle is greater than that of the combined flat fan nozzle, and the maximum velocity of the flat nozzle is greater than that of the combined flat fan nozzle.

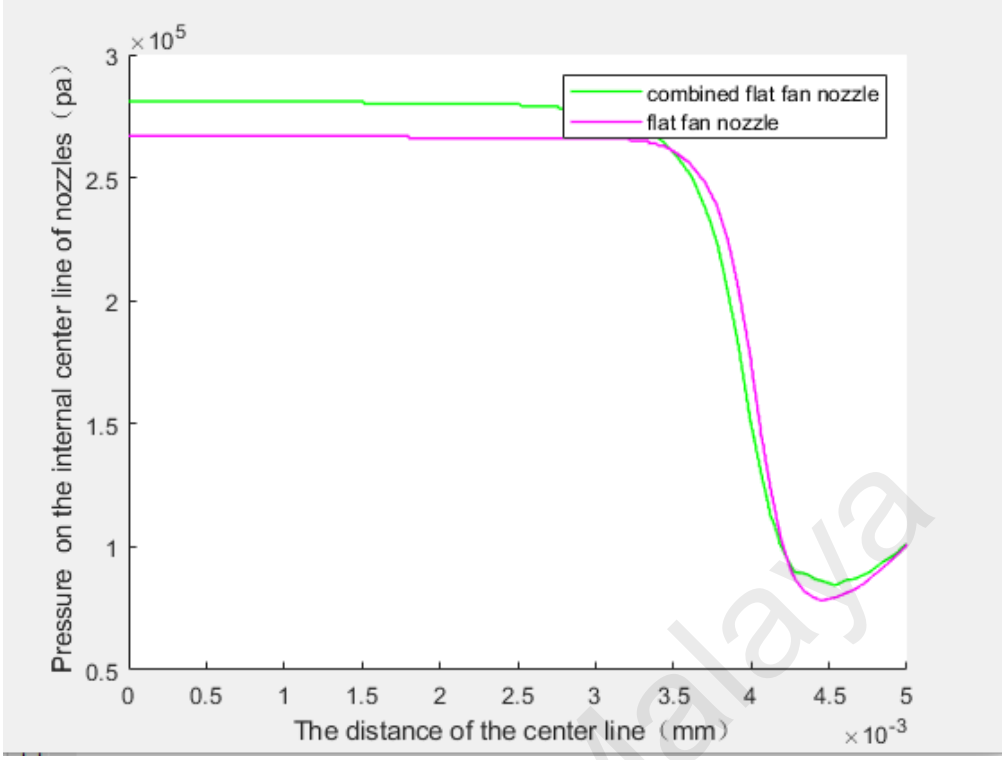

Figure 4.49: The center line fluid pressure curve of 2 nozzles

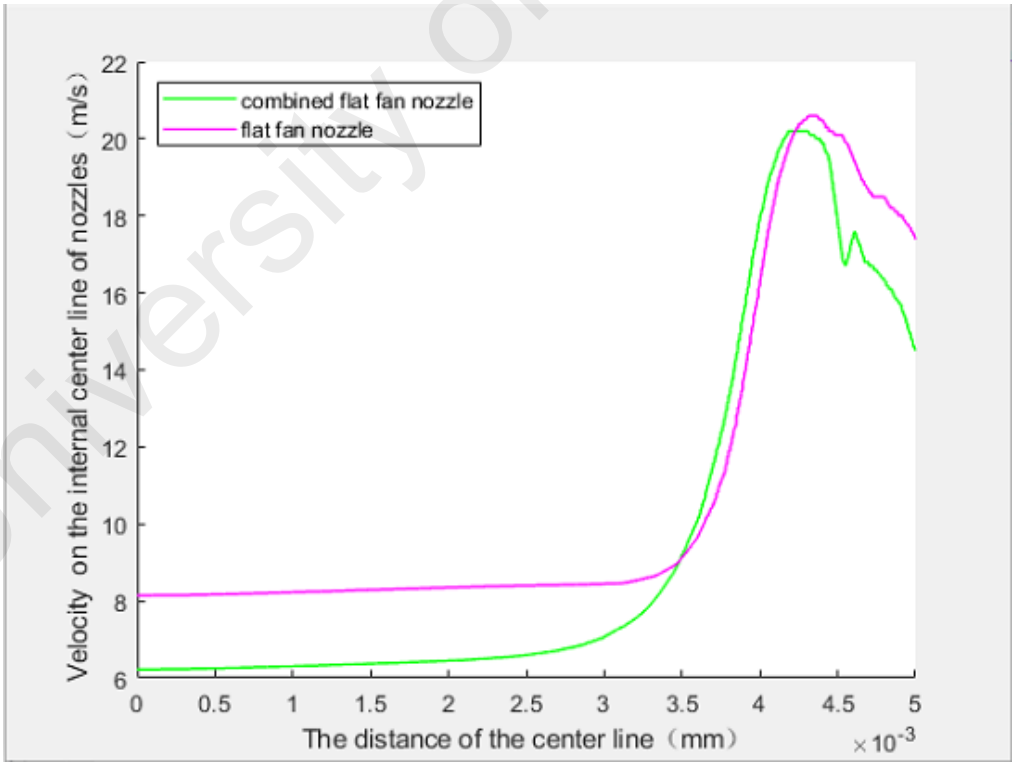

Figure 4.50: The center line fluid velocity curve of 2 nozzles

The spray velocity of the flat fan nozzle is slightly higher than the combined flat fan nozzle. The spray shape causes the uneven spray and the different size of the spray

droplets (Zhang Ji, 2013). The combined nozzle is more common, and the mist distribution effect is better (Fan Qingni, 2010).

CHAPTER 5: CONCLUSIONS AND FUTURE WORK

5.1 Conclusions

This paper uses ANSYS FLUENT software to simulate the internal fluid flow of 13 combined fan flat nozzles with different parameter models, then compares the fluids flow of flat and combined flat fan nozzles with the same parameters, and draws the following conclusions:

1. The most important factor influencing the spray velocity of the nozzle are grooving angle, followed by the diameter of the cavity and lastly the length of the throat. The main parameter that affects the spray range is the grooving angle. The main parameters that affect the mass flow of liquid are grooving angle and cavity diameter. Comprehensively considered, the atomization performance of the nozzle is the best when the grooving angle is 35°, the diameter of the cavity is 3mm and the length of the throat is 2mm. It provides the basis for the design, optimization, and improvement of UAV spraying pesticide device nozzle in the future.

2. The groove of the nozzle is the key part of the fluid flow velocity and pressure change. Changing the main structural parameters of the nozzle for comparative analysis provides a reference for the reasonable selection of the structural parameters of the nozzle. The nozzle groove is the turning point of pressure and velocity changes. The velocity difference and pressure change between the droplets and the air are important reasons for the further tearing and thinning of the droplets, so the manufacturability of the groove is very important.

3. Under the same main parameters, the spray shape of the flat fan nozzle is not concentrated, and the spray velocity is not uniform. But the spray velocity is faster than

the combined fan nozzle. The spray range of the combined flat fan nozzle is smaller than that of the flat fan nozzle, but the spray is more concentrated and uniform.

5.2 Future work

This paper simulates the internal flow of combined fan nozzles with different structural parameters used in low-altitude UAV pesticide spraying devices. Due to the limitation of theoretical knowledge and time, the following improvements are hoped in future research:

1. This study only has a direct impact on the nozzle atomization performance within a certain range of nozzle throat length, cavity diameter, and grooving angle. Therefore, in the future, researchers can compare and analyze the influence degree of each structural parameter on its performance parameter in a larger range.

2. This study only performed a simulation analysis on the performance of the combined flat fan nozzle and flat fan nozzle with one structural parameter. There is an opportunity to simulate a variety of structural parameters of the flat fan nozzles in the future.

3. The simulation results of ANSYS FLUENT are not the same as the actual situation. The effect of nozzle parameters on spray performance can be analyzed with real nozzles and other equipment and instrument measurements.

CHAPTER 6: REFERENCES

Acquavella JF, A. B. (2004, 3). Glyphosate Biomonitoring for Farmers and Their Families: Results from the Farm Family Exposure Study. *Environ Health Perspect* , pp. 321-326.

Augustyn, A. (2011, 2 15). Retrieved from The Editors of Encyclopaedia Britannica: https://www.britannica.com/science/Bernoullis-theorem

Burguete J, P. E. (2003). Improving drop size and velocity estimates of an optical disdrometer: implications for sprinkler irrigation simulation. *Transaction of the ASABE*, 2103-2116.

Diaphragm pump. (2008, 10). Retrieved from Wikipedia: https://en.wikipedia.org/wiki/Diaphragm_pump

Fan Qingni, Z. H. (2010). *Research status of traditional nozzle.* Proceedings of Forestry Machinery Development Forum under the New Situation.

Fan Rong, Y. F. (2016). Research on the Series Type Spectrum Model of Fan-shaped Fog Nozzle in Plant Protection. *Shanxi Agricultural University School Newspaper*, 36-37.

Garcerá C, M. E. (2017). Spray pesticide applications in Mediterranean citrus orchards: Canopy deposition and off-target losses. *Science of the Total Environment*, 599-600.

Hanjalic, K., & Launder. (1972). A Reynolds stress model of turbulence and its application to thin shear flows. *Journal of Fluid Mechanics*, 609-638.

Holshouser, D. (2013, 7 2). Application Equipment for Effective Insect Pests and Foliar Disease Control. *Equipment Technology*, 11-12.

Huang, F. (2014). *Parametric design of nozzle for plant protection.* NWAFU.

Huijiang, S. (2011, 3). Research on Atomization Characteristics of Fan-shaped Nozzle. *Continuous casting*, pp. 31-33.

JENSEN, J. (2019). Agricultural Drones: How Drones Are Revolutionizing Agriculture and How to Break into this Booming Market. *UAV coach*, 1-2.

Jiang Fan, H. P. (2008). *Fluent advanced application and case analysis.* Beijing: Tsinghua University Press.

Jianming, C. (2005). *Spray theory.* Beijing: Machinery Industry Press.

Junhua, H. (2018). *Simulation and Experimental Research on Performance* . Simulation and Experimental Research on Performance .

Kearney GD, X. X. (2015, 1 20). Assessment of Personal Protective Equipment Use Among Farmers In Eastern North Carolina: A Cross-Sectional Study. *Agromedicine*, pp. 43-54.

Langtry R B, M. F. (2009). Correlation-Based Transition Modeling for Unstructured Parallelized Computational Fluid Dynamics Codes. *Aiaa Journal*, 2894/2906.

Lesmes Fabian C, T. S. (2014, 3 1). Evaluation Of Models For Dermal Exposure Assessment in Farming Systems in Developing Countries. p. 1.

Li Xu, W. C. (2000, 4). Design of low-flow fan spray nozzle. *Journal of Agricultural Machinery*, pp. 38-41.

LORRIC. (1991). *PRODUCT NOZZLE*. Retrieved from LORRIC: http://www.lorric.com.cn/Products/Nozzles

Lu Xiaolan, F. X. (2011). Influence of spray technical parameters on droplet drift characteristics. *Journal of Agricultural Machinery*, pp. 13-14.

Mourin, R. R. (2002). *Pesticide Action Network Asia and the Pacific (PAN AP).* Penang, Malaysia: P.O. Box.

Organization, U. N. (2003). Guidelines for minimum requirements for pesticide application equipment. In Rome, *Portable (operator carry) spray machine* (pp. 87-91). FAO.

Ou Qibin, H. Z. (2016, 10). Comparative analysis of finite element stress of helicopter wings based on Solidworks and ANSYS. *mechanical*, pp. 31-35.

Pedlosky, J. (1987). Geophysical fluid dynamics. Springer.

Pimentel, D. (2013). Amounts of Pesticides Reaching Target Pests: Environmental Impacts. pp. 49-51.

Pingzeng, L. (2007). *Development of a precision test bench for comprehensive performance of nozzles and research on performance of fan spray nozzles.* Nanjing Agricultural College.

PNR Italia. (2017). Retrieved from PNR spray nozzle for industrial applications: http://www.pnr.eu/prodotti/j/

Qingni, F. (2011). *Research on Pesticide Atomization System of Small Unmanned Helicopter.* Nanjing : Nanjing Forestry University.

RaoMogili, U. (2018). Review on Application of Drone Systems in Precision Agriculture. *Procedia Computer Science*, 502-509.

Shariff FM, R. A. (2008, 8 2). Chemical Weed Control in the Oil Palm Sector with Particular Reference to Smallholders and Nursery Operators. *Oil Palm Industry Economic Journal*, pp. 29-38.

Snelder DJ, M. M. (2008). Risk Assessment of Pesticide Usage by Smallholder Farmers In The Cagayan Valley. *Crop Prot*, pp. 747-762.

Sun Wenfeng, W. L. (2009, 11). Analysis of factors affecting spray quality of boom sprayer[J]. *Agricultural Mechanization Research*, pp. 114-117.

Supplies, p. (2018, 10 13). *Sprayer Pump Types, Costs, and Specifications*. Retrieved from SPRAYER SUPPLIES: https://www.sprayersupplies.com/sprayer-pump-guide

Tan Luke, H. Z. (2014). The Dilemma and Enlightenment of UAV Development. pp. 1660-1664.

Thompson J C, R. J. (2007). The atomization of viscoelastic fluids in flat-fan . *Journal of Non-Newtonian Fluid Mechanics*, 11-22.

United States Environmental Protection Agency. (2018, 4 2). Retrieved from Basic Information about Pesticide Ingredients: https://www.epa.gov/ingredients-used-pesticide-products/basic-information-about-pesticide-ingredients

Vikrant Suryawanshi, A. J. (2019). *Design & Development of Agricultural Fertilizer Spraying Drone with Remote Controller and Autonomous Control with low weight Aluminium Alloy frame Structure.* Maharashtra, India: Department of Electronics

and Telecommunication, Annasaheb Dange College of Engineering & Technology.

Wang Bin, Y. H. (2016). Development status and trends of drone spraying technology. *Agriculture and Technology*, 59-62.

Wang Yanping, C. Y. (2009). Design and Simulation of Plant Protection UAV Sprinkler. *Mechanical Engineering of Chengdu Institute of Technology*, pp. 51-53.

Wilcox, D. C. (2008). Formulation of the k-omega Turbulence Model Revisited. *AIAA Journal*, 2823-2838.

Wiles-Purdue, K. (2020, 7 1). SOLUTION TO VISCOSITY MYSTERY MAY CURB PESTICIDE POLLUTION. *Physical Review Letters*.

Xiang, L. (2014). *Research on the high-pressure jet characteristics of the fan nozzle.* Southwest Jiaotong University.

Xinyu Xue, Y. L. (2016). Develop an unmanned aerial vehicle based automatic aerial spraying system. *Computers and Electronics in Agriculture*, 58-66.

Y. Huang, W. C. (2009). *Development of a spray system for an unmanned aerial vehicle platform.* St. Joseph, Michigan: Published by the American Society of Agricultural and Biological Engineers.

Yang Xuejun, Y. H. (2005). Experimental research on fan spray nozzle. *China Agricultural Mechanization*, 39-42.

Yang, J. (2012, 3). Experimental research on spray uniformity of spray machinery[J]. *Hunan Agricultural Machinery*, pp. 55-60.

Yanmis. (2019, 10 24). *amazon*. Retrieved from Diaphragm Pump 12V, Food Grade Diaphragm Pump Self Priming 12V Mute Water Pump: https://www.amazon.co.uk/Diaphragm-Pump-Grade-Priming-Water/dp/B07ZHK5CK8

Youlin, X. (2009). *Research on Plant Protection Mechanical Mixer and Its Pesticide Online Mixing Performance.* Nanjing: Nanjing Forestry University.

Zhai Enyu, Z. J. (2013). Development of a Test-bed for Measuring Wear of Hydraulic Nozzle. *China Agricultural Machinery Chemistry News*, 189-193.

Zhang Ji, M. H. (2013). Application of Simulation Technology in the Experiment of Narrow Slot Nozzle Atomization Characteristics. *Journal of Shandong Agricultural University*, 122-126.

Zhang Xinming, L. Q. (2012). *Numerical simulation of the influence of structure parameters of high-pressure water fan nozzle on internal flow field.* Chongqing: School of Power Engineering, Chongqing University.